Newsletters on Stratigraphy, Vol. 46/3 (2013), 339–361 **Article**
Stuttgart, October 2013

An expanded lower Eocene shelf sequence from the eastern Aquitaine Basin, SW France: biostratigraphy, biofacies, and stable carbon and oxygen isotopes

Claudius M. Pirkenseer[1], Etienne Steurbaut[2,5], Hemmo A. Abels[3], Chris King[4], and Robert P. Speijer[5]

With 11 figures and 3 tables

Abstract. The early Eocene is characterized by a succession of orbitally-controlled global stable carbon isotope excursions, with some being linked to climatic and related biotic perturbations. The impact of these isotopic excursions has been primarily studied in deep-sea sections under comparably stable conditions. In order to investigate the impact of global post-PETM isotopic signals on shallow marine settings, the Ypresian neritic 'Blue Marls' of the Corbières (SW France) were investigated. High-resolution records of microfossil biota and stable carbon and oxygen isotopes pinpoint biostratigraphic, paleoecologic and geochemic constraints. Calcareous nannofossil biostratigraphy positions the sequence in the upper part of zone NP11, possibly ranging into basal NP12, which is conformable with larger benthic foraminifera data indicating shallow benthic zone SBZ8. This implies a time span of about 0.4 Myr and high overall sedimentation rates of about ~32 cm/kyr for the section. A shallowing upward trend from outer neritic to coastal settings is observed in the development of the lithostratigraphy and the microfossil assemblage. The assemblages can be subdivided in seven larger biofacies and four ostracod assemblage zones. The lower third of the section is characterized by strongly fluctuating and partly high plankton/benthos-ratios for neritic settings. A final pronounced peak in plankton occurrence is associated with strong decrease of benthic biota, suggesting anoxic conditions in the outer neritic environment. Several local negative $\delta^{13}C$- and $\delta^{18}O$-excursions can be identified in the section. The upper, most pronounced and consistent negative $\delta^{13}C$ excursion is tentatively linked to global carbon isotope excursion K (ETM3) based on the biostratigraphic constraints.

Key words. biostratigraphy, neritic, Ypresian, stable isotope excursions, biofacies, ETM3, Corbières

Authors' addresses:
[1] Department of Geosciences, Unit Earth Sciences, University of Fribourg, Chemin du Musée 6, CH-1700 Fribourg, Switzerland. E-Mail: claudiusmarius.pirkenseer@unifr.ch
[2] Royal Belgian Institute of Natural Sciences, Paleontology, Vautierstraat 29, BE-1000 Brussels, Belgium. E-Mail: etienne.steurbaut@naturalsciences.be
[3] Department of Earth Sciences, Utrecht University, Budapestlaan 4, NL-3584 The Netherlands. E-Mail: h.a.abels@uu.nl
[4] 16A Park Rd., Bridport, DT6 5DA, UK
[5] Department of Earth & Environmental Sciences, KU Leuven, Celestijnenlaan 200E, BE-3001 Heverlee-Leuven, Belgium. E-Mail: robert.speijer@ees.kuleuven.be
Corresponding author: Claudius Pirkenseer, Department of Geosciences, University of Fribourg, Chemin du Musée 6, CH-1700 Fribourg, Switzerland. E-Mail: claudiusmarius.pirkenseer@unifr.ch

www.borntraeger-cramer.de
DOI: 10.1127/0078-0421/2013/0037
0078-0421/2013/0037 $ 5.75

1. Introduction

The late Paleocene and early Eocene are characterized by a steady increase in mean global ocean temperature as reflected in the $\delta^{18}O$ record, leading to the Early Eocene Climatic Optimum (EECO) during the Ypresian (Zachos et al. 2001, 2005). This interval is also characterized by a series of pronounced, short-lived negative $\delta^{13}C$ excursions (Cramer et al. 2003). The Paleocene-Eocene Thermal Maximum (PETM) is the most pronounced of these carbon isotope excursions (e.g. Bowen et al. 2006) and is believed to be triggered by an abrupt, massive input of isotopically-light carbon into the exogenic atmosphere-ocean carbon pool (Zachos et al. 2005, Dickens 2009, Dunkley Jones et al. 2010).

The marine impact of a global climatic event close to the Paleocene/Eocene-boundary was documented during the late 1980s and early 1990s (e.g. Thomas 1989, Thomas et al. 1990, Kennett and Stott 1991), and became known as the Benthic Extinction Event (e.g., Schmitz et al. 1996) or Benthic Foraminiferal Extinction Event (e.g. Pardo et al. 1999). Since then the effects of the PETM on foraminiferal faunas have been widely discussed affecting both benthic and planktic taxa (e.g. Canudo and Molina 1992, Speijer et al. 1995, 1996, Schmitz et al. 1996, Thomas 2003, Ernst et al. 2006, Petrizzo 2007, Alegret et al. 2010), with widespread extinctions in the benthic record and assemblage shifts among the planktic foraminifera. The influence of the PETM on middle to outer neritic benthic foraminifera (Speijer et al. 1995, 1996, Dupuis et al. 2003, Ernst et al. 2005, Alegret and Ortiz 2006, Stassen et al. 2012) and ostracoda (Speijer and Morsi 2002, Morsi et al. 2011) has mainly been documented for the Tethyan region, with few exceptions (Stassen et al. 2012).

Marine data on post-PETM hyperthermals however are much less common and generally limited to geochemistry (e.g. Cramer et al. 2003, Lourens et al. 2005, Stap et al. 2009, Galeotti et al. 2010), with few exceptions reporting biotic responses (Egger et al. 2005, Agnini et al. 2009, Dedert et al. 2012, Stassen et al. 2012).

So far, most marine studies on Eocene hyperthermal events focus on pelagic/hemipelagic sediments (e.g. Nicolo et al. 2007, Agnini et al. 2009, Stap et al. 2009, Galeotti 2010), avoiding terrestrial or regional influence that alters the geochemical signal and faunal record.

This study aims at generating a high-resolution benthic microfossil and stable isotope record in the Early Ypresian neritic shelf environments of the Corbières ('Blue Marls' Formation, Aude, SW France) in order to track paleoecologic changes within a shallowing-up sequence, to specify the regional biostratigraphic context and to record the occurrences and ranges of insufficiently documented, characteristic early Eocene ostracod taxa. The interpretation of the biostratigraphic data and the stable isotope signature of the Pradelles-en-Val section, the target studied herein, and its correlation to the deep-sea standard isotope records

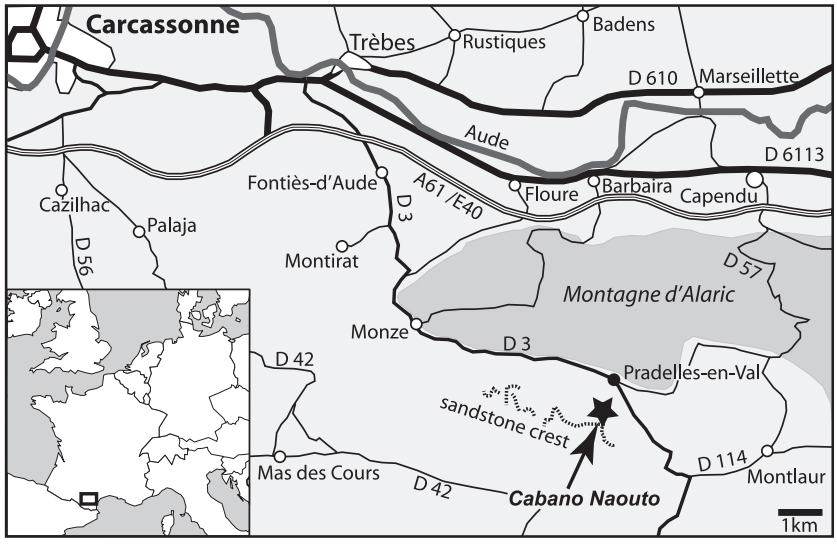

Fig. 1. Outcrop location in southwestern France (modified from openstreetmap.org).

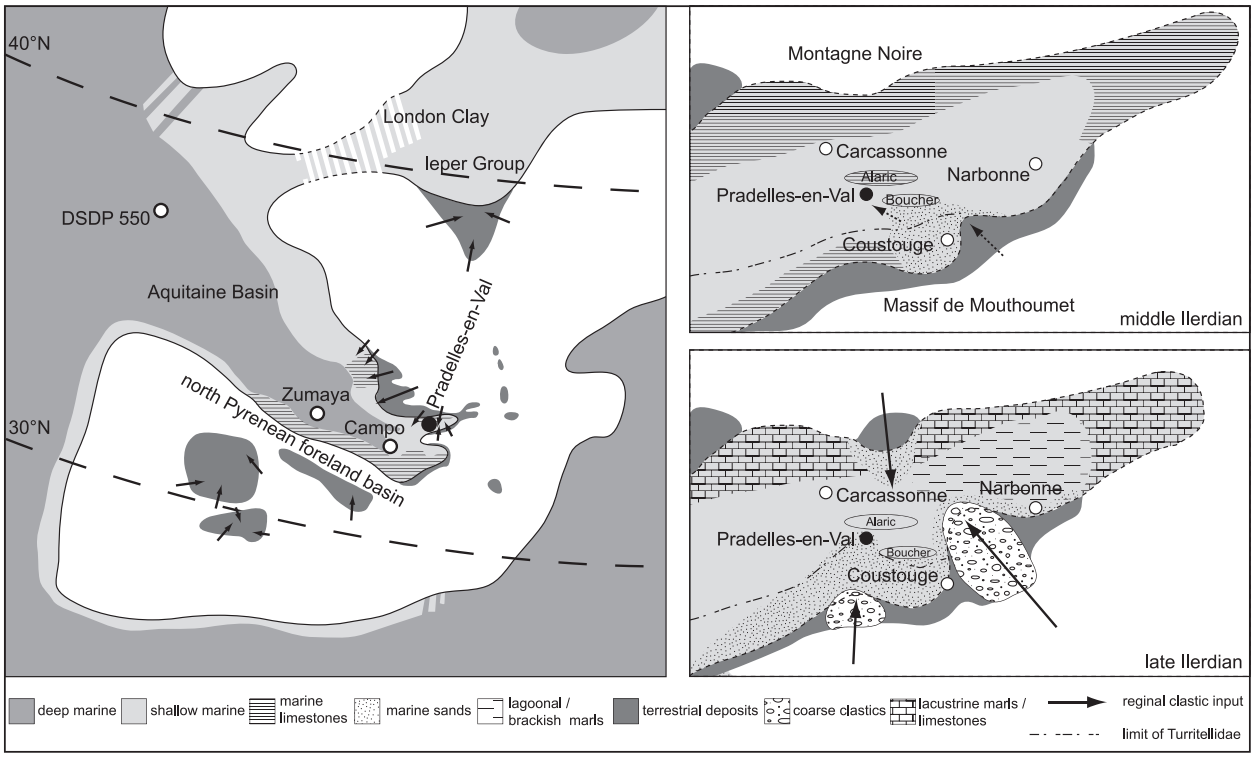

Fig. 2. Paleogeographic situation of western Europe during the Ypresian and local basin evolution (assembled from Plaziat 1981, Meulenkamp et al. 2000, Gély and Sztrákos 2000, Martín-Martín et al. 2001 and field data).

may allow accurate positioning of this section in the Geologic Time Scale 2012 and unravel of environmental change in a neritic setting during early Eocene global warming.

2. Regional geologic and stratigraphic overview

2.1 The Ilerdian as regional subdivision

The Ilerdian and Cuisian have restricted significance, being essentially based on the evolutionary stages of shallow larger benthic foraminiferal taxa (LBF) and conceptually compromised by an imprecisely defined lower boundary of the Cuisian. The Ilerdian, as used here, encompasses the shallow benthic foraminiferal zones SBZ5-9 of Serra-Kiel et al. (1998). In the latter context the Ilerdian and Cuisian are present in the Geological Time Scale 2012 (Vandenberghe et al. 2012). The subdivision of the Ilerdian in lower, middle and upper parts corresponds to the succession of shallow benthic foraminiferal assemblage intervals, SBZ5-6, SBZ7-8 and SBZ9, respectively (Molina et al. 1992, Serra-Kiel et al. 1998, Molina et al. 2003). The onset of the Ilerdian has been proposed to be simultaneous with the onset of the Paleocene-Eocene Thermal Maximum (PETM) and, consequently, with the base of the Eocene (Scheibner et al. 2005, Pujalte et al. 2009, Scheibner and Speijer 2009; Fig. 8).

However, since most papers on Tethyan early Eocene neritic facies use the 'regional' Ilerdian and Cuisian instead of the standard and more comprehensive Ypresian stage (e.g. Martín-Martín et al. 2001, Molina et al. 2003, Rasser et al. 2005, Scheibner et al. 2007), the terminology is included in the stratigraphic discussion of this paper.

2.2 Geologic setting and paleogeographic development

South-south-west of the village of Pradelles-en-Val an extended section of the early Eocene 'Blue Marls' crops out on the northern slope of the 'Cabano Naouto' sandstone ridge (Fig. 1).

The Corbières-Minervois foreland basin (Fig. 2) is pinched between the Massif de Mouthoumet (south, active margin) and the Montagne Noire (north, passive

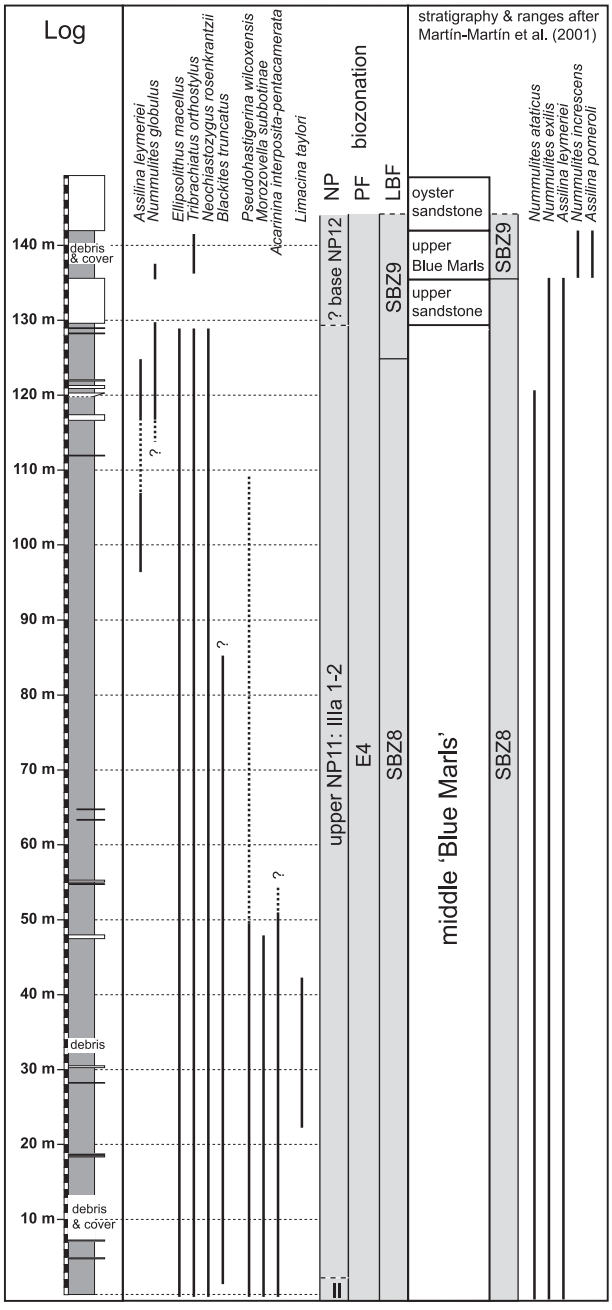

Fig. 3. Lithostratigraphy, biostratigraphic zones (LBF = larger benthic foraminifera, PF = planktic foraminifera, NP = calcareous nannoplankton) and ranges of biostratigraphically important taxa of the Pradelles section (occurrences of LBF partly from Massieux 1973) in comparison (thickness not equivalent) with the regional stratigraphic synthesis in Martín-Martín et al. (2001).

margin; Martìn-Martìn et al. 2001). Marine sedimentation within the Corbières-Minervois-Basin started in the Early Thanetian, when the North-Pyrenean trough progressed eastward, overstepping the Lannemezan High (Gély and Sztrákos 2000), resulting in the development of several transgression-regression cycles during the Late Thanetian and the Ypresian (Plaziat 1981, Tambareau et al. 1995, Scheibner et al. 2007). During the middle Ilerdian, the North-Pyrenean Foreland Basin experienced accelerated subsidence (Gély and Sztrákos 2000), leading to deeper depocenters and succeeding a rather shallow sedimentation of widespread platform limestones (Tambareau 1994, Rasser et al. 2005, Scheibner et al. 2007).

At the base of the middle Ilerdian several hundred meters of marine sediments accumulated throughout the Minervois, Montlaur and Talairan synclines (second and third sequence of Martín-Martín et al. 2001; Fig. 8). A comparable thickness was deposited in similar sections to the southwest in the Tremp Basin (Molina et al. 2003). In the late Ilerdian accommodation space decreased and terrigenous sediments prograded mainly from the passive southern margin (Plaziat 1981, Martín-Martín et al. 2001, Fig. 2), with superposition of post-Ilerdian continental deposits.

2.3 Previous biostratigraphic investigations on the "Blue Marl" Formation of the Corbières

The first comprehensive biostratigraphic analysis of the Corbières region was published in Lezaud et al. (1969). The 'Nummulitique' or Blue Marls of the Corbières were attributed to the Ypresian on the basis of calcareous nannofossil and planktic foraminiferal data. This study gave the impetus for a more systematic investigation of these 'Blue Marls', which lasted up to the late 1980s. Consequently, they figure in many compilation works on Mediterranean biostratigraphy (Massieux 1973, Kapellos and Schaub 1973, Schaub 1981, Breton and Vizcaïno 1997, amongst others) and paleogeography (Plaziat, many publications synthesized in 1981). The only recent regional biostratigraphic data available, based on a series of 12 samples from different localities, allow the lower to middle 'Blue Marls' to be attributed to NP10 at the base and to NP10-11 interval at the top, and the upper 'Blue Marls' to NP11-12 (Martín-Martín et al. 2001). The investigation of the large benthic foraminifera (LBF) in several other adjacent outcrops allowed to identify Zone SBZ8 in the middle 'Blue Marls' and the 'upper

sandstone', and Zone SBZ9 in the upper 'Blue Marls'. These low-resolution data are largely consistent with the data presented here.

3. Material and methods

About 150 m of marine Ilerdian sediments are accessible in the vicinity of the village of Pradelles-en-Val (Fig. 3). From 0 to 116.3 m, the succession is made up of uniform dark grey marls with rare, 5 to 30 cm thick, intercalated sandstone beds. Above 116.3 m, the marls become increasingly sandy, and the sandstone beds more abundant and thicker with higher carbonate content, before culminating in two massive sandstone banks of about 6 to 7 m thickness (Fig. 3). The sandstone beds in the lower part of the section contain abundant plant debris and exhibit load casts and current marks. The latter indicates a general SSE to NNW directed paleocurrent. The marls show no structure, except some bioturbation and small pyritic nodules.

127 samples (PEV1-13, CN0-115) were taken from a fresh surface at 1 m stratigraphic resolution. The general SSW 15° dip of the layers is corrected for the thickness estimate. Due to the topography of the outcrop, the sampling had to be carried out along a series of closely spaced consecutive subsections (for section breaks and related GPS coordinates see Table 1).

Marl chunks were dried at 50 °C in order to obtain dry weights of 600 to 800 gr per sample level. Multiple soaking of the material in soda leach (75 g Na_2CO_3/1000 ml H_2O) achieved the breakdown of the tough marls. For the final cleaning the residues were mixed with pure Rewoquat W3690PG and water for 24 hours. The residue was then washed through a 63 µm-mesh sieve and finally dry-sieved (630/250/180/125/63 µm) and picked. 630 µm- and 250 µm-fractions were screened entirely to obtain a complete overview of the biota larger than 250 µm. Ostracods were picked entirely from this fraction. In general, the preservation ranges from poor to moderate showing re-crystallization and abrasion. The calcareous nannofossils present a similar type of preservation, marked by selective dissolution and re-crystallization.

Bulk samples for isotopic analyses were dried at 50 °C. Carbonate powders were reacted with 100 % phosphoric acid (density > 1.9; Wachter and Hayes 1985) at 75 °C using a Kiel III online carbonate preparation line connected to a ThermoFinnigan 252 mass spectrometer in the isotope laboratory at GeoZentrum Nordbayern. All values are reported in per mil relative to the V-PDB standard by assigning a $\delta^{13}C$ value of +1.95‰ and a $\delta^{18}O$ value of −2.20‰ to the NBS19 reference material. Reproducibility was checked by replicate analysis of laboratory standards and is smaller than ± 0.08‰ (95 % uncertainty range).

Plankton/miliolid/endobenthic/epibenthic-ratios were calculated from the 125 µm-fraction by counting 300 specimens per sample. The taxa selected as 'endobenthic' include *Pseudouvigerina*, buliminids, bolivinids, *Reophax*, *Lagenammina*, *Ammobaculites* and nodosariids against a background of mostly epibenthic rotaliids as *Cibicides*, *Karreria*, *Pulsiphonina* and *Gyroidinoides*.

Qualitative and quantitative calcareous nannofossil investigations have been carried out on smear-slides from 25 samples almost equally spaced along the section, following standard procedures as described in Steurbaut and King (1994). About two square centimeters of glass-slide have been examined for each sample at 1000 × or 1250 × magnification. The taxonomy adopted here is essentially from Perch-Nielsen (1985), the biozonation relates to Steurbaut (1991, 1998), which is a refinement of Martini's (1971) standard nannofossil zonation.

Calcareous nannofossil material is stored in the collections of the Royal Belgian Institute of Natural Sciences (RBINS, Brussels, Belgium), sample residues at the Department of Earth & Environmental Sciences of KU Leuven (Belgium), and picked microfossils at the Unit Earth Sciences of the University of Fribourg (Switzerland).

Table 1 GPS coordinates of samples and position of log relocation.

GPS (sample)	N	E	Height
PEV13	43° 08.322′	02° 30.818′	227 m
CN0	43° 08.288′	02° 30.841′	230 m
CN36	43° 08.234′	02° 30.843′	248 m
CN58	43° 08.206′	02° 30.826′	270 m
CN102	43° 08.179′	02° 30.788′	305 m
CN103	43° 08.138′	02° 30.850′	322 m
CN112	43° 08.029′	02° 30.841′	295 m

between PEV13 and CN0 log relocation 70 m SSE
between CN102 and CN103 log relocation 120 m SE
between CN111and CN112 log relocation 120 m S

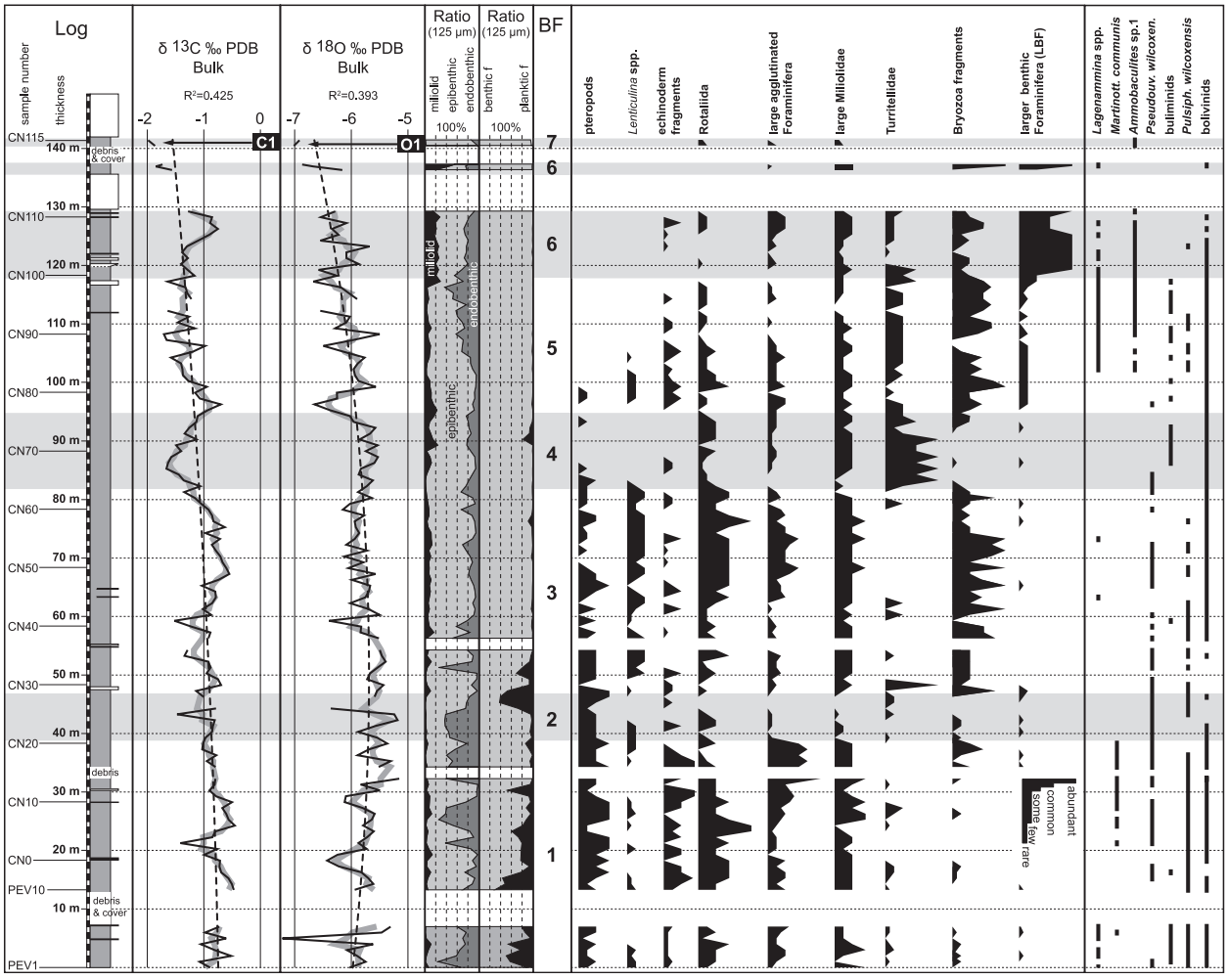

Fig. 4. Relative abundance range chart and range chart of characteristic biota > 250 µm (BF = biofacies), foraminiferal ratios (125 µm-fraction) and stable isotope bulk sediment values (black line, three point moving average = gray line, dashed line = polynomial 2-order trendline). The alternance of gray/white areas indicates the extent of the individual biofacies, C1-3 and O1-3 mark consistent stable isotope minima.

4. Results

4.1 Biostratigraphy (Fig. 3)

The co-occurrence of *Tribrachiatus orthostylus* (up to 128.3 m), *Ellipsolithus macellus* (consistently up to 68.3 m and recurrence at 89.3 m and 128.3 m) and *Neochiastozygus rosenkrantzii* (up to 128.3 m), in combination with the absence of *Discoaster lodoensis*, indicates calcareous nannoplankton zone NP11 throughout the 130 m thick well exposed part of the section. The 7 m thick marl unit intercalated between the two massive uppermost sandstone layers cannot be accurately dated because of the absence of the marker species *E. macellus*, *N. rosenkrantzii* and *D. lodoensis*. However, it is probably still part of upper NP11 as not a single additional marker of NP12, known from mid-latitudes, such as *Aubrysphaera deconinckii*, *Micrantholithus mirabilis*, *Helicosphaera* taxa etc., has been recorded. However an assignment to basal NP12 cannot be excluded. *Blackites truncatus*, which is also recognized throughout most of the section (except for the lowermost sample PEV1 and the uppermost 30 m), allows a more precise biostratigraphic positioning. A comparative study of the nannofossil data from Belgium (Steurbaut 1998), Denmark (Schmitz et al. 1996) and Kazakhstan (Steurbaut 2011) shows that the LO (lowest occurrence) of *B. truncatus* can be pinpointed in the upper part of NP11, at the base of nannofossil zone III of Steurbaut (1991, 1998). The lowermost

sample PEV1 might represent the top of the underlying nannofossil zone II. Summarizing, the Pradelles-en-Val section covers the upper part of NP11, with an uncertainty for the uppermost marl, which might belong to the base of NP12. Consequently, the Pradelles-en-Val section is of lower to middle Ypresian age.

The planktic foraminifera of the Pradelles-en-Val section consist of generally long-ranging species such as *Acarinina pseudotopilensis*, *A. wilcoxensis*, *Pseudohastigerina wilcoxensis* and *Morozovella subbotinae*. Poor preservation and small size render further determination of acarininid taxa difficult. Based on the simultaneous occurrence of *Pseudohastigerina wilcoxensis* and *Morozovella subbotinae* as well as the absence of *M. aragonensis* the sediments of the lower part of the Pradelles-en-Val section (HO *M. subbotinae* at 41.3 m) fall within the biostratigraphic range base E2 – top E4 (early to middle Ypresian; Berggren and Pearson 2006, Wade et al. 2011). The additional taxa *Acarinina esnaensis*, *A. coalingensis* and *A. soldadoensis* as recorded in Massieux (1973) indicate comparable ranges (P4 – E5/7). The presence of the short ranging *A. aspensis* (base E7) and the Paleocene *A. nitida* as reported in Massieux (1973) is not confirmed in our material.

The LBF (large benthic foraminifera) assemblages from the upper part of the Pradelles-en-Val section include *Nummulites globulus* and *Assilina leymeriei* (conform to the occurrences in Massieux 1973), the marker species of shallow benthic zone SBZ8 ('middle Ilerdian 2'; Serra-Kiel et al. 1998).

The planktic gastropod ("pteropod") taxon *Limacina taylori* is documented from the interval between 22.3 to 42.3 m, representing the first record outside the North Sea Basin. This species characterizes the pteropod-zone 7 in Janssen and King (1988) that is correlated with nannofossil zone NP11, though it also rarely occurs in the subsequent pteropod-zones 8 and 9. Assuming the occurrence of *Limacina taylori* represents the acme distinguishing pteropod-zone 7, the lower part of the Pradelles-en-Val section is accordingly attributed to this zone.

4.2 Stable isotopes record

Bulk sediment isotopic values for $\delta^{13}C$ and $\delta^{18}O$ show alternation between –1.98 to –0.45‰ for $\delta^{13}C$ and –7.22 to –5.15‰ for $\delta^{18}O$ (V-PDB) in the Pradelles-en-Val section (Fig. 4 and 5). There is a gradual 0.7‰ negative long-term shift in bulk $\delta^{13}C$ values towards the upper part of the section. The long-term bulk $\delta^{18}O$ isotope curve shows a positive trend of about 0.3‰ on average in its lower end and a negative trend of about 1‰ in its upper end, changing between 40 and 60 m (see trend lines in Fig. 4, 6).

The stable carbon isotope record shows less short-term variability than the oxygen isotope record. In the oxygen isotope record, most fluctuations on short time scales occur in the lower (0 to 44.3 m) and in the upper third (93.3 to 129.3 m) of the section. This high-frequency variability occurs with periods mostly 2 to 4 m, causing most cycles being represented by two to four data points due to sample resolution. No clear robust regular short-term cyclicity is therefore observed. In line with that, the small-scale variability does not show consistent cyclicity between the oxygen and the carbon records. This suggest that either the sampling resolution of 1 m has not been high enough to depict this variability sufficiently or no clear high-frequency variability occurred in the isotope records of the section. Additionally it probably indicates that a diagenetic overprint did not take place, as is also shown by the random distribution of isotopic values in the cross plot (Fig. 5).

Several relatively negative oxygen isotope excursions stand out from the short-term variability. The strongly negative value at 5 m is represented only by one sample, and thus ignored as aberrant outlier. The first excursion is the least prominent, ranges from

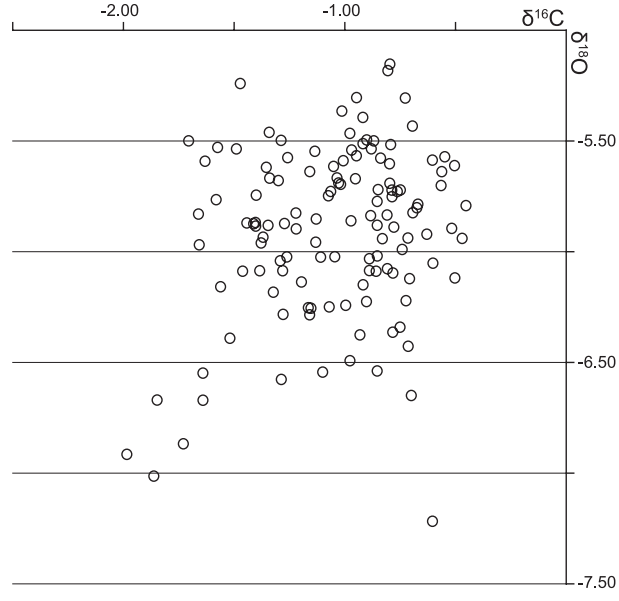

Fig. 5. Bulk sediment stable carbon and oxygen isotope cross plot.

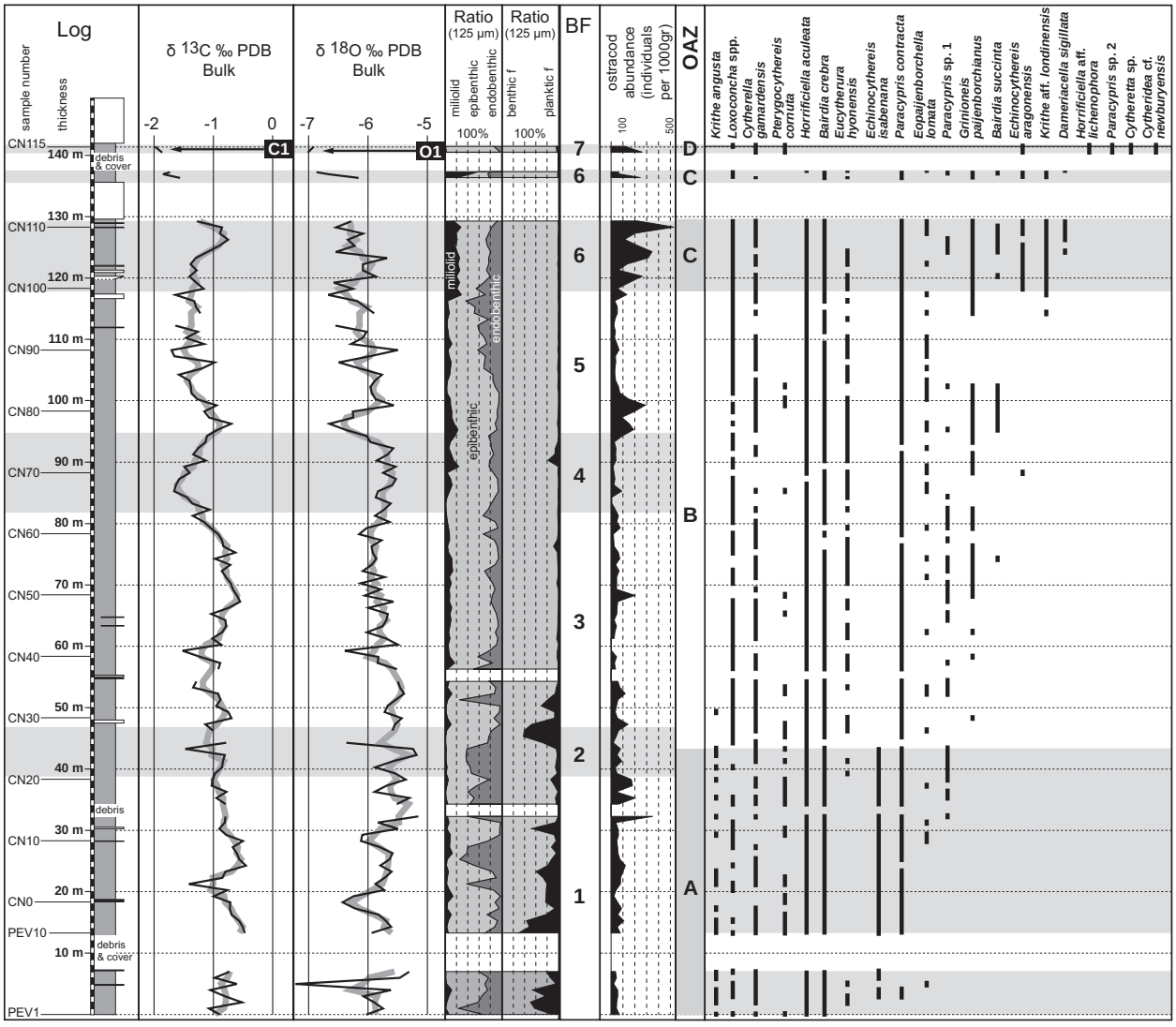

Fig. 6. Ostracod range chart (BF = biofacies, OAZ = ostracod-assemblage-zone), foraminiferal ratios (125 µm-fraction) and stable isotope bulk sediment values (black line, three point moving average = gray line). The alternation of gray/white areas indicates the extent of the individual BF or OAZ, C1-3 and O1-3 mark the more pronounced stable isotope minima.

14.3 to 23.3 m, and is characterized by an excursion of ~0.6‰, while the second ranges from 92.3 to 99 m with an excursion of ~0.9‰. The more pronounced negative excursion between 123.3 m and 140.5 m is labeled O1 and shows a decrease of about 1.3‰.

The first carbon isotope excursion occurs from 13.3 to 23.3 m with a decrease of ~0.7‰, the second from 75.3 to 96.3 m with an excursion of ~0.9‰, and the most pronounced labeled C1 starts at 126.3 m and shows a decrease of 1.2‰ (Fig. 4, 6). Only the labeled excursions C1 and O1 occur coincidently and seem thus to stand out from background variability.

Longer-term variations are visible in the carbon isotope record in depicting minimal values at meter ~20, meter 45–60, meter ~85, meter 108–120, and meter 140. In the oxygen isotope series, lows at ~18, ~95, and ~117 meter alternate with highs at ~12 m, ~25 m, 30–52 m, ~85 m, ~102 m and ~122 m. These patterns in oxygen and carbon isotope series do not match each other (except for the uppermost part of the section), similar to the lack of match of the short-term variability. Time-series analysis on these series does not help detecting the high-frequency cyclicity since this is not depicted properly in the record, as discussed above, nor the low-frequency cyclicity be-

cause only few not very consistent nor regular cycles occur.

4.3 Biota and biofacies (Fig. 4, 6–7)

4.3.1 Biofacies

The bioclast fraction above 250 µm is essentially composed of pteropods, other gastropoda, echinodermata, bryozoa, ostracoda, larger benthic foraminifera (LBF) and several large-sized benthic foraminiferal groups (e. g. miliolids, agglutinated taxa, *Lenticulina*). Analysis of the distribution patterns of these different bioclast groups has led to the identification of seven different biofacies (BF).

BF1 is characterized by relatively high P/B ratios and abundant occurrences of pteropods, echinoderm fragments, rotaliid foraminifera, large agglutinated foraminifera and miliolids. Levels of reduced benthos are intercalated. In BF2 benthos is greatly reduced (substantial decrease in large miliolid and agglutinated foraminifera), hinting towards dysoxic to anoxic conditions, especially in levels 44.3 to 46.3 m, which are dominated by pteropods. BF3 is dominated by rotaliid foraminifera and bryozoa, with *Lenticulina* spp., large miliolids and agglutinated foraminifera being abundant. In BF4 turritellid gastropods are dominant, while other benthos and pteropods, except large miliolids, are greatly reduced. BF5 is largely comparable to BF3, except for the larger benthic foraminifera, which are for the first time consistently represented, and the pteropods and *Lenticulina* spp., which disappear in the lower half of BF5. LBF become the dominant faunal component in BF6, while the distribution of the other biota is comparable to that in BF5. Finally, in BF7, benthic life is greatly reduced, except for some rotaliid, agglutinated and miliolid foraminifera. Turritellid gastropods, bryozoa and LBF, which are dominant in BF6 are entirely absent in BF7.

4.3.2 Characteristics of bioclasts, foraminifera and ratios

Pteropods (planktic gastropods) occur exclusively as pyritised moulds. Bryozoan fragments indicate the presence of a large variety of morphogroups from flat discoidal (*Lunulites*) to thinly branched forms. Relatively large rotaliid foraminifera are represented mostly by the genera *Gyroidinoides*, *Karreria* and *Cibicides*. Large agglutinated foraminifera comprise mainly the genera *Sabellovoluta*, *Martinottiella*, *Textularia* and *Spiroplectinella*. Large, poorly preserved *Cyclofo-rina* are continuously present in the section. Most gastropods belong to the family Turritellidae.

Foraminifera in the 125 µm size fraction consist mainly of small bolivinids, *Pulsiphonina wilcoxensis*, *Pseudouvigerina wilcoxensis* and small agglutinated foraminifera of the genera *Ammobaculites*, *Lagenammina* and *Reophax*. Endobenthic taxa show strongly variable values, but are rather abundant in BF1-2. High endobenthic ratios plot generally antagonistic trends to high plankton ratios. In BF3 endobenthic values generally stay below 30 %. The increased occurrence of small agglutinated foraminifera in BF5 and BF6 is expressed in raised endobenthic ratios. The lower half of the section (BF1 to BF3) is marked by small miliolid ratios of less than 20 %, with average values around 10 %. In the uppermost part of BF5, the values abruptly increase to 28 % and remain high throughout BF6. The ratio drops to 0 % in BF7.

BF1 shows a variable, generally medium-high plankton/benthos-ratio that decreases towards its top. A pronounced plankton peak occurs in the upper BF2 where larger benthos is nearly absent, with values reaching 63 %. It is essentially made up by small subbotinids and globoturborotaliids. Plankton peaks in the lower part of the section contain mainly several species of *Acarinina* (e. g., *Acarinina wilcoxensis*) and *Pseudohastigerina wilcoxensis*. In the upper two thirds of the section (lower BF3-7) the P/B-ratio drops to 1–2 %. A single exception is the 8–19 % peak in levels 90.3 to 92.3 m, characterized by the dominance of large *Subbotina roesnaesensis*.

4.3.3 Ostracoda

A total of 26 ostracod taxa are recorded. The ranges of the most common species are recorded on Fig. 6. The cumulative abundance of ostracods shows extended acmes in the upper part of BF1, the base of BF5 and in BF6. Ostracod abundance is generally low during intervals with high ratios of planktic foraminifera.

Four ostracod assemblage zones are identified on the basis of the ranges and frequencies of characteristic species. The top of the lowermost Zone OAZ-A, defined by the highest occurrence of *Echinocythereis isabenana*, is located on level 44 m. OAZ-B is characterized by the common occurrences of *Paracypris contracta* and *Grinioneis paijenborchianus* and ranges from 44 to 118.3 m. OAZ-C is marked by the acme of *Krithe* aff. *londinensis* and common occurrences of *Echinocythereis aragonensis* and *Grinioneis paijenborchianus*. OAZ-C records the highest diversity of the section (15 taxa). *Dameriacella sigillata* is restricted to

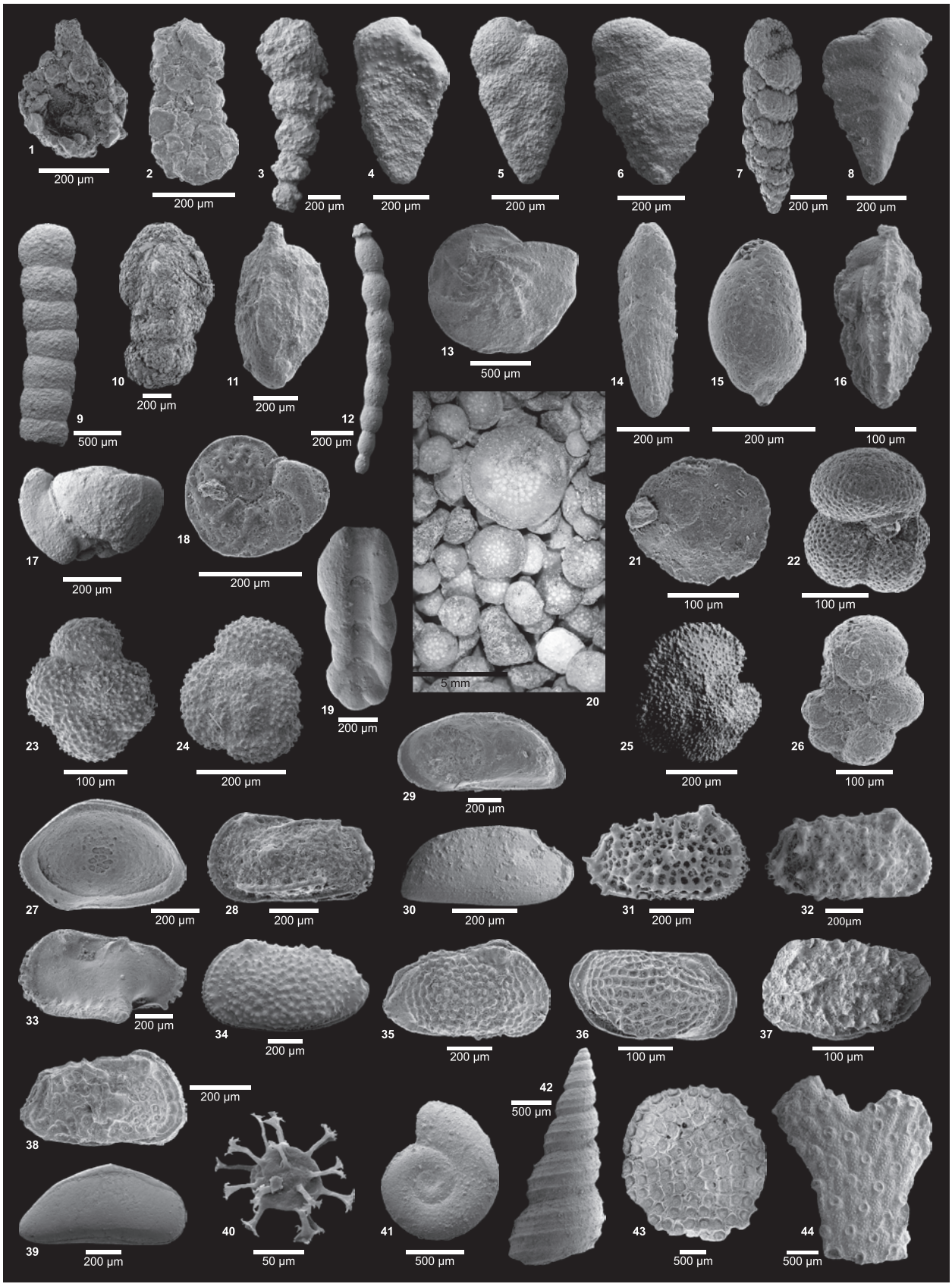
1
200 µm
2
200 µm
3
200 µm
4
200 µm
5
200 µm
6
200 µm
7
200 µm
8
200 µm
9
500 µm
10
200 µm
11
200 µm
12
200 µm
13
500 µm
14
200 µm
15
200 µm
16
100 µm
17
200 µm
18
200 µm
19
200 µm
5 mm
20
21
100 µm
22
100 µm
23
100 µm
24
200 µm
25
200 µm
26
100 µm
27
200 µm
28
200 µm
29
200 µm
30
200 µm
31
200 µm
32
200µm
33
200 µm
34
200 µm
35
200 µm
36
100 µm
37
100 µm
38
200 µm
39
200 µm
40
50 µm
41
500 µm
42
500 µm
43
500 µm
44
500 µm

the upper part of this zone. The uppermost OAZ-D is distinguished on the basis of a strong assemblage shift. Several characteristic taxa of preceding OAZ disappear, and previously not recorded species (e.g. *Horrificiella* aff. *lichenophora*) occur for the first time.

The most common species, *Horrificiella aculeata* and *Bairdia crebra*, range throughout the section, except for the topmost 1.5 m thick OAZ-D zone. Further long-ranging taxa include *Paracypris contracta*, *Loxococoncha* ex gr. *subovata*, *Cytherella gamardensis*, *Pterygocythereis cornuta* and *Eucytherura hyonensis*. *Krithe angusta* has its topmost occurrence at 49.3 m, in the lower part of OAZ-B.

4.3.4 Calcareous nannofossils

The Pradelles-en-Val section is marked by poorly preserved, low-diversity calcareous nannofossil associations (maximum of 18 species), dominated by small Prinsiaceae (essentially *Toweius*) and *Coccolithus pelagicus*. The number of specimens fluctuates throughout the section, although remains always low (less than 15 specimens/field of view), pointing to a paleoenvironment, which was not very suitable for nannoplankton productivity and/or selective dissolution of coccoliths on the seafloor. The high sedimentation rates may also have played a role in the development of these low concentrations. The Pradelles-en-Val sequence shows a generally decreasing diversity and strongly increasing ratio of reworked Cretaceous taxa (10 to 100 %). However, some subtle differences are recorded allowing a subdivision in four assemblage groups. Assemblage group A (base section to CN61 at ~80 m) includes the quantitatively and qualitatively richest associations of the section, although remaining low (between 15 and 10 specimens/field of view), and with rather low Cretaceous reworking (< 10 % of the specimens). Group B (up to CN93 at ~111 m) shows reduction to 50 % of the number of specimens/field of view (~5 spec.) and a major increase in reworked Cretaceous forms (over 50 %). The associations in group C (CN106-113 or from 125 to ~137 m) present a higher species diversity than these in group B, notwithstanding the same number of specimens per field of view, and are characterized by a substantial increase in *Toweius* spp. and a decrease in reworked Cretaceous forms (to ~30 %). Calcareous nannofossils are extremely rare (1 to 2 specimens/field of view) in the topmost interval (CN114-115 at 140-141 m), and essentially represented by Cretaceous taxa (over 85 % up to 99 % in the topmost sample). *Toweius* taxa are the only autochthonous component in this group D.

5. Discussion

5.1 Lithostratigraphy

The biostratigraphic and log data of the Pradelles-en-Val section presented here allow a close correlation with the regional lithologic units described in Martín-Martín et al. (2001). Levels 0 to 129.7 m (BF1-5) represent the middle 'Blue Marls'. The interval from 116 to 129.7 m forms a transitional zone consisting of solidified marls with increasing sand content, followed

Fig. 7. Characteristic fossil taxa of the Pradelles-en-Val section. 1. *Lagenammina* sp. (90.3 m); 2. *Ammobaculites midwayensis* Plummer, 1933 (108.3 m); 3. *Reophax* cf. *scorpiurus* de Montfort, 1808 (7.0 m); 4. *Siphotextularia concava* (Karrer, 1868) (6.0 m); 5. *Karreriella* cf. *cubensis* Cushman & Bermudez, 1937 (5.0 m); 6. *Textularia* cf. *pseudogramen* Chapman & Parr, 1937 (5.0 m); 7. *Textularia plummerae* Lalicker, 1935 (87.3 m); 8. *Spiroplectinella plummerae* (Cushman, 1948) (38.3 m); 9. *Martinottiella communis* (d'Orbigny, 1846) (38.3 m); 10. *Sabellovoluta* sp. (35.3 m); 11. *Cycloforina* cf. *lippa* (Le Calvez, 1946) (52.3 m); 12. *Dentalina* sp. (6.0 m); 13. *Lenticulina* sp. (104.3 m); 14. *Loxostomoides applini* (Plummer, 1927) (108.3 m); 15. *Globobulimina ovata* (d'Orbigny) *cowlitzensis* (Beck, 1943) (59.3 m); 16. *Pseudouvigerina wilcoxensis* Cushman & Ponton, 1932 (24.3 m); 17. *Gyroidinoides girardanus* (Reuss, 1851) (38.3 m); 18. *Cibicidoides* cf. *praecursorius* (Schwager, 1883) (59.3 m); 19. *Karreria fallax* Rzehak, 1891 (38.3 m); 20. LBF, predominantly *Assilina leymerii* (Archiac & Haime 1853) (119.3 m); 21. *Pulsiphonina wilcoxensis* (Cushman, 1927) (45.3 m); 22. *Subbotina roesnaesensis* (90.3 m); 23. *Acarinina pentacamerata* (Subbotina, 1947) *-interposita* (Subbotina, 1953) (25.3 m); 24. *Acarinina wilcoxensis* (Cushman & Ponton, 1932) (47.3 m); 25. *Morozovella subbotinae* (Morozova, 1939) (24.3 m); 26. *Pseudohastigerina wilcoxensis* (Cushman & Ponton, 1932) (108.3 m); 27. *Bairdia crebra* Deltel, 1962 (87.3 m); 28. *Grinioneis paijenborchianus* (Keij, 1957) (90.3 m); 29. *Krithe* aff. *londinensis* (126.3 m); 30. *Krithe angusta* Deltel, 1962 (42.3 m); 31. *Horrificiella aculeata* (Bosquet, 1852) (85.3 m); 32. *Horrificiella* aff. *lichenophora* (Bosquet, 1852) (140.3 m); 33. *Pterygocythereis cornuta* (Roemer, 1838) (35.3 m); 34. *Echinocythereis isabenana* Oertli, 1960 (38.3 m); 35. *Echinocythereis aragonensis* Oertli, 1960 (123.3 m); 36. *Loxoconcha* cf. *subovata* (v. Muenster, 1830) (46.3 m); 37. *Eucytherura hyonensis* Keij, 1957 (108.3 m); 38. *Dameriacella sigillata* Liebau, 1991 (128.3 m); 39. *Paracypris contracta* (Jones, 1852) (47.3 m); 40. dinocyst (24.3 m); 41. pteropod (38.3 m); 42. Turritellidae indet. (90.3 m); 43. *Lunulites* cf. *bugei* (102.3 m); 44. Bryozoa indet. (38.3 m).

by the massive calcareous sandstone layer known as the 'upper sandstone' (containing *Nummulites globulus*; Massieux 1973). Based on the abrupt disappearance of *Assilina leymeriei* in sample CN107 (middle of BF6; Fig. 3) the base of SBZ9 can be lowered slightly in comparison to Martín-Martín et al. (2001). The top of the section is characterized by the succession of the upper 'Blue Marls' and the subsequent calcareous 'oyster sandstone'. Both sandstone units are supposed to be deposited within a short time span.

5.2 Paleoecology (Fig. 11, Table 2)

Biofacies (BF) 1 represents a fully marine outer neritic environment as indicated by the common occurrence of abundant planktic foraminifera, pteropods, ostracoda (e. g. *Bairdia crebra*, *Echinocythereis isabenana*, *Krithe angusta*) and benthic foraminifera taxa (e. g. *Gyroidinoides girardanus*, *Pulsiphonina wilcoxensis*, *Pseudouvigerina wilcoxensis*).The nearly continuous presence of bioturbation, benthic/endobenthic foraminifera, echinoderms and small crabs indicates generally well-oxygenated bottom conditions throughout this part of the section. The decreasing abundance of most benthos in BF2 and its near absence in levels 44.3 to 46.3 m, in combination with the pronounced peak of plankton abundance, points towards oxygen depletion (e. g. Bernhard 1986, Tyson and Pearson 1991, Moodley and Hess 1992, Levin 2003). The decrease of pteropod and planktic foraminifera, as well as the nearly simultaneous disappearance of the ostracod *Krithe angusta* at the base of BF3, indicates a shift to middle neritic conditions.

BF4 is dominated by turritellid gastropod fragments, suggesting the proximity of shallower, high nutrient soft-bottoms, possibly delta-front settings (Dominici and Kowalke 2007, Waite and Strasser 2010), which is corroborated by the strong increase of reworked Cretaceous nannofossils. The total disappearance of planktic foraminifera and pteropods, the continued high levels of reworked Cretaceous nannofossils and the start of the consistent occurrence of assilinids and nummulitids in BF5 point to a futher shallowing of the depocenter. In BF6 rather small (2–7 mm diameter) LBF (mainly *Assilina* and *Nummulites*) dominate, with fragments of bryozoans, echinoderms and abundant small miliolids co-occurring. Geel (2000) attributes comparable assemblages from southeastern Spain to the (inner) shallow shelf under normal marine conditions. The shift from high miliolid/LBF-ratios in BF6 to a miliolid/LBF-free and middle neritic ostracod assemblage in BF7 indicates the recurrence of a more open marine setting despite the near absence of autochthonous plankton, relating to the transgression of the 4th sequence in Martìn-Martìn et al. (2001). A transition to a nearshore, probably brackish environment is indicated by the presence of coastal faunal elements in the subsequent "oyster sandstones".

Table 2 Biofacies classification and main characteristics.

Biofacies	Basic characteristics
1.	**fully marine, outer neritic**; abundant benthic and planktic foraminifera, ostracoda, pteropods, brachiopoda, echinodermata, bioturbation
2.	**marine, dysoxic to anoxic**; strongly reduced benthos, dominance of plankton
3.	**fully marine, middle neritic**; decrease of plankton
4.	**marginal marine, possibly delta front**; dominance of turritellid gastropods, increase of reworked Cretaceous nannoplankton
5.	**fully marine, inner neritic**; near absence of plankton, Bryozoa, continuous occurrence of larger benthic foraminifera
6.	**fully marine, inner neritic to lagoonal**; dominance of larger benthic foraminifera, abundance of small miliolid foraminifera
7.	**fully marine, middle neritic**; absence of larger benthic foraminifera, recurrence of a more open marine ostracod assemblage

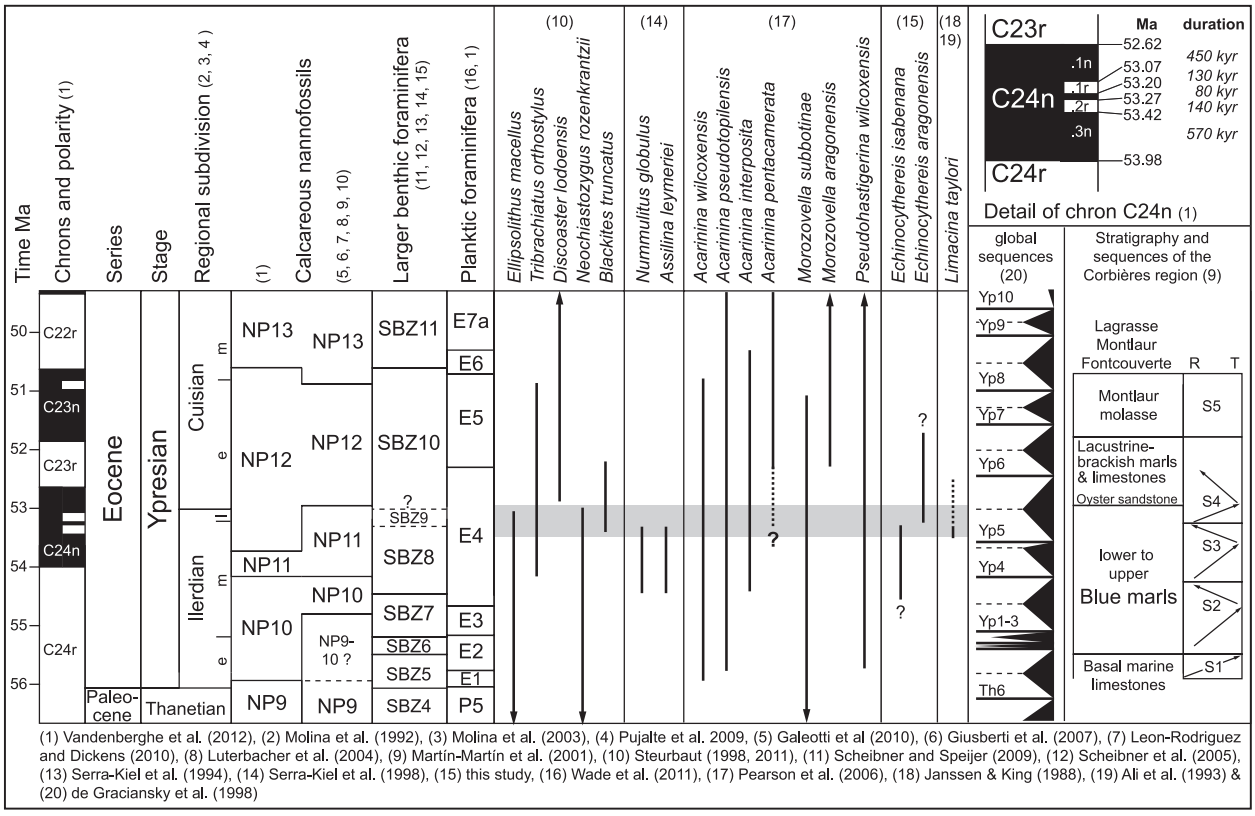

(1) Vandenberghe et al. (2012), (2) Molina et al. (1992), (3) Molina et al. (2003), (4) Pujalte et al. 2009, (5) Galeotti et al (2010), (6) Giusberti et al. (2007), (7) Leon-Rodriguez and Dickens (2010), (8) Luterbacher et al. (2004), (9) Martín-Martín et al. (2001), (10) Steurbaut (1998, 2011), (11) Scheibner and Speijer (2009), (12) Scheibner et al. (2005), (13) Serra-Kiel et al. (1994), (14) Serra-Kiel et al. (1998), (15) this study, (16) Wade et al. (2011), (17) Pearson et al. (2006), (18) Janssen & King (1988), (19) Ali et al. (1993) & (20) de Graciansky et al. (1998)

Fig. 8. Stratigraphic chart and biozonation of the early Eocene, ranges of biostratigraphically important taxa and lithostratigraphic units/sequences of the Corbières region. The grey area denotes the biostratigraphic extent of the Pradelles section.

5.3 The temporal framework (Fig. 8)

5.3.1 Interpretation and discrepancies

Since the last decade much improvement has been achieved in calibrating different geochronologies. However there is still an ongoing discussion concerning the correlation of the radio-isotopic with the astronomic age model (e. g. the so-called 50 and 60 Ma discrepancies as discussed in Vandenberghe et al. 2012). Furthermore, Westerhold et al. (2012) recently proposed 3 options for the onset of the PETM based on astronomical calibration, with a best fit of "option 1" (PETM at 55.530 ± 0.05 Myr) for very-long eccentricity cycle minima. This implies a shift of the absolute age calibration of one 405 kyr cycle relative to the combined age model presented in Vandenberghe et al. (2012) (which correlates accordingly to "option 2" in Westerhold et al. 2012). However, since the absolute duration of and the distance between early Eocene CIEs remains consistent in all three options of Westerhold et al. (2012), there are no immediate implications for our study, as the timespan recorded in the Pradelles-en-Val section lies within this interval. Hence in the present paper we adopt the combined age model for the Paleogene as proposed in Vandenberghe et al. (2012) for the calibration of biostratigraphic tie-points.

The position of the calcareous nannofossil zones is adopted from Luterbacher et al. (2004), taking into account the recent adjustments by Giusberti et al. (2007), Galeotti et al. (2010) and Leon-Rodriguez and Dickens (2010). The upper boundary of NP11 is placed accordingly close to the middle of Chron C24n.1n.1n and its lower boundary in the lower part of Chron C24r (Galeotti et al. 2010). These tie-points, which were established in a series of deep-sea sections worldwide, are consistent with the data recorded from the shelf settings in the southern North Sea Basin (Steurbaut 1998) and at Aktulagay in Kazakhstan (Steurbaut 2011): lowest occurrence of *D. lodoensis* (marker of base NP12) in middle of Chron C24n.1n (= C24AN in Steurbaut 1998), and lowest consistent occurrence of this taxon (LCO or FCO) in its top. However, the boundaries of nannoplankton zone NP11 are significantly different as presented in Vandenberghe et al.

(2012) (see Fig. 8). Since the data for correlation of nannoplankton zones in the timescale has been derived from localities in the Pacific, we adapted the aforementioned previous (European and Atlantic) data to the new combined age model of Vandenberghe et al. (2012). The exact positioning of the lower boundary of NP10, defined by the lowest occurrence (LO) of *Tribrachiatus bramlettei*, has been a major point of discussion and debate, because very rare occurrences are known to occur clearly before the start of its consistent occurrence. However, most authors are currently agreeing that the very first *T. bramlettei* appear within the upper part of the PETM (Agnini et al. 2009, Galeotti et al. 2010). The calibration of the shallow benthic zones (SBZ) of Serra-Kiel et al. (1998) with the standard planktic biozonations has also been controversial. The position of Zone SBZ9, which is identified in the top of the Pradelles-en-Val section, has been shifted over the years, from uppermost NP11 – base NP12 (Serra-Kiel et al. 1998), to exclusively lower NP12 (Martin-Martin et al. 2001, Vandenberghe et al. 2012) up to a position spanning the NP10–NP11 boundary (Afzal et al. 2009).

The latter and subsequent age tie points are estimated from the combined age model in Vandenberghe et al. (2012) (Fig. 8). According to the data in the North Sea Basin and Aktulagay (Steurbaut 1998, 2011) the LO of *Blackites truncatus* has been pinpointed close to the base of nannozone IIIa, which is in the upper part of Chron C24n.2r (equivalent of C24AR in Steurbaut 1998, 2011) at ~53.29 Ma. The HO of *Assilina leymeriei*, the marker for SBZ8, has been recorded within the middle of Biofacies 6 in the Pradelles-en-Val section (this study, Massieux 1973). This means that the major part of the marls, up to CN107, is still within SBZ8. The HO of *Ellipsolithus macellus*, which in the North Sea Basin (Steurbaut 1998) and at Aktulagay (Steurbaut, 2011) defines the top of nannozone IIIa2 and almost coincides with the base of NP12, is recorded in CN110, indicating that the topmost part of the middle blue marls below the lower massive sandstone ("upper sandstone", Fig. 3) is still within NP11. This implies that the top of the middle blue marls is within the lower middle of Chron C24n.1n at ~52.90 Ma. It also suggests that the base of SBZ9 is still within NP11, as was initially put forward by Serra-Kiel et al. (1998).

Pteropod-zone 7 (Janssen and King 1988) ranges from lower part Chron C24n.2r to basal Chron C24n.3n. It thus correlates well with the nannofossil data from the lower part of the Pradelles-en-Val section.

Generally poor preservation limits the use of planktic foraminifera for biostratigraphic interpretation. For instance the occurrence of *Acarinina pentacamerata* (E5-7) in the lower part of the section contradicts the nannoplankton age dating (upper NP11 which is within E4). However, Berggren et al. (2006) mentioned the uncertainty concerning the total range of *A. pentacamerata* as well as the gradual morphologic transition from the resembling ancestral taxon *A. interposita* (E4-6). Small acarininid specimens resembling the two latter taxa are documented in the lower Pradelles-en-Val section.

The acme of larger *Subbotina*, associated with a short increase in P/B ratio at 90.3 m, may represent an extra tie-point allowing refinement of the temporal framework during which the deposition of the blue marls at Pradelles-en-Val took place. *Subbotina* blooms are known to occur at a similar stratigraphic position in Belgium (the "*Globigerina patagonica*" acme-zone of Willems 1982 = *Subbotina* interval of King 1991) and Kazakhstan (Aktulagay section: King et al., in press). In several Ypresian sections in Belgium there is a sharp increase in planktic foraminifera, essentially *Subbotina*, in a very thin interval (25 cm with very high planktic foraminiferal ratios of over 50 %, at the base of the about 3 m thick *Subbotina*-dominated interval with PF ratios between 5 and 10 %, Steurbaut pers. com.), at the transition of nannofossil zones IIIa1 and IIIa2. This level is located within the lower part of Chron C24n.1n at approximately 53.05 Ma (see Fig. 8).

The upper boundary of the ostracod assemblage zone OAZ-A is defined by the species shift of *Echinocythereis isabenana* to *E. aragonensis-posterior*. Oertli (1960) placed this speciation event in the early Lutetian. Molina et al. (2003), when revising the stratigraphy of the Tremp and Campo sections, positioned this species transition in NP10. Thus, the value of the *E. isabenana* to *E. aragonensis-posterior* transition as a (regional) biostratigraphic marker event is questionable and needs further investigation.

5.3.2 Sedimentation rates

From the tie points discussed in 5.3.1 it can be concluded that the major part of the Pradelles-en-Val section from close to the base to 129.3 m, representing about 125 m of sediment, has been deposited within a timespan of approximately 390 kyr. An average sediment accumulation rate of about 32.1 cm/kyr can be computed for the whole section, corresponding roughly to the upper limit of other regional values. The intermediate tie-point of the *Subbotina* acme allows the

detection of differences in sedimentation rates within the lower Blue Marls: lower 86 m in 240 kyr, the upper 39 m in 150 kyr. Accumulation rates in the upper third (26.0 cm/kyr) of the section are accordingly lower than those in the lower two thirds (35.8 cm/kyr), despite the increased influx of coarser sediments from BF6 onwards. Accumulation rates in the topmost 20 m of the section ("Upper Sandstone", upper "Blue Marls" and "Oyster Sandstone") are difficult to evaluate due to the lack of calibration points.

Very high sediment accumulation of ~200–300 m within nannoplankton zone NP11 (duration of ~1.2–1.4 myr; Luterbacher et al. 2004, Galeotti et al. 2010; see Fig. 8) is registered in the region (Massieux 1973, Martín-Martín et al. 2001), increasing up to 500 m in similar paleoenvironmental settings in the Tremp and Campo area to the southwest (Molina et al. 1992, Serra-Kiel et al. 1994). Judging from the biostratigraphic and lithostratigraphic data recorded in Martín-Martín et al. (2001) from neighbouring sections in the Corbières and the approximate duration of nannoplankton zone NP11 regional average sediment accumulation rates are estimated at 14–25 cm/kyr for the middle 'Blue Marls'.

5.4 Stable Isotopes

5.4.1 Authenticity of the local stable carbon and oxygen isotope signal

The pronounced sharp negative shift located in the lower part of BF4, coincides with a strong increase of turritellid gastropods, but without any change in $\delta^{18}O$ values. High relative abundance of Turritellidae indicates nutrient/organic-rich, probably delta-front sediments. The latter hints towards an increased freshwater influx and in-situ burial of excess organic and reworked terrestrial matter in BF4. This is corroborated by the increase of reworked Cretaceous nannofossils. The incorporation of buried negative organic carbon during diagenetic carbonate re-precipitation due to the closed nature of the marly sediments (e.g. Marshall 1992) probably leaves the pronounced negative $\delta^{13}C$ imprint on the bulk sediment as recorded in BF4. Unaltered recent and fossil marine gastropod shells display $\delta^{13}C$ and $\delta^{18}O$ values higher than recorded in the bulk samples of BF4 (e.g. Andreasson and Schmitz 1996, 2000, Latal et al. 2004). Since the shells only contribute about 0.5 to 5‰ to the entire sample mass, the geochemic imprint of gastropod shells on the bulk sample is negligible, which is evidenced by the negative isotopic trend in BF4.

Though bryozoa, turritellid gastropods and LBF represent the most common faunal elements in BF3-6, only LBF contribute significantly to the bulk sediment mass in BF6. Values for early to middle Eocene LBF from western India vary between –1.0 to 1.2‰ $\delta^{13}C$ and –4.7 to –2.9‰ $\delta^{18}O$ (Saraswati et al. 1997). Seasonal variability recorded from one Lutetian nummulite species from southern England ranges between 0.5 to 2.5‰ $\delta^{13}C$ and –5.7 to –1.2‰ $\delta^{18}O$, with lower values recorded from summer periods (Purton and Brasier 1999). On average these values are much higher than those documented in the bulk curves in BF6. The period of low $\delta^{13}C$ values starts 15 m down-section (in BF4) of the mass occurrence of LBF,

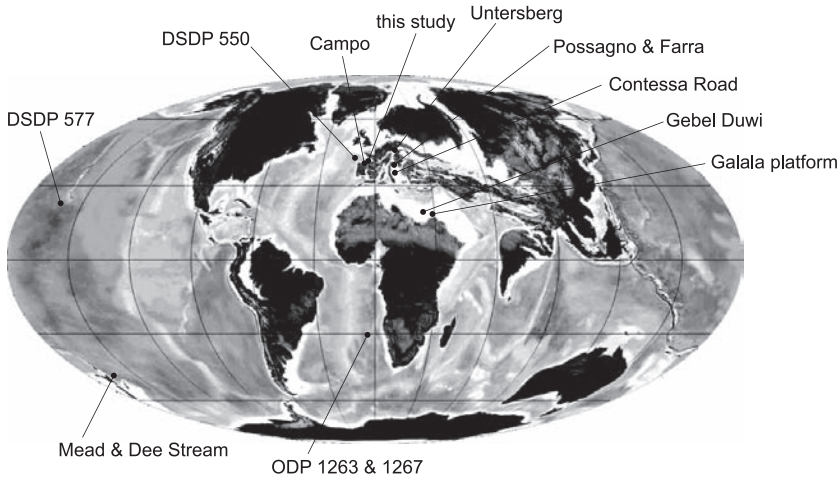

map modified from Blakey: http://jan.ucc.nau.edu/~rcb7/50moll.jpg

Fig. 9. Paleogeographic position of cited localities recording Carbon Isotope Excursions (CIEs).

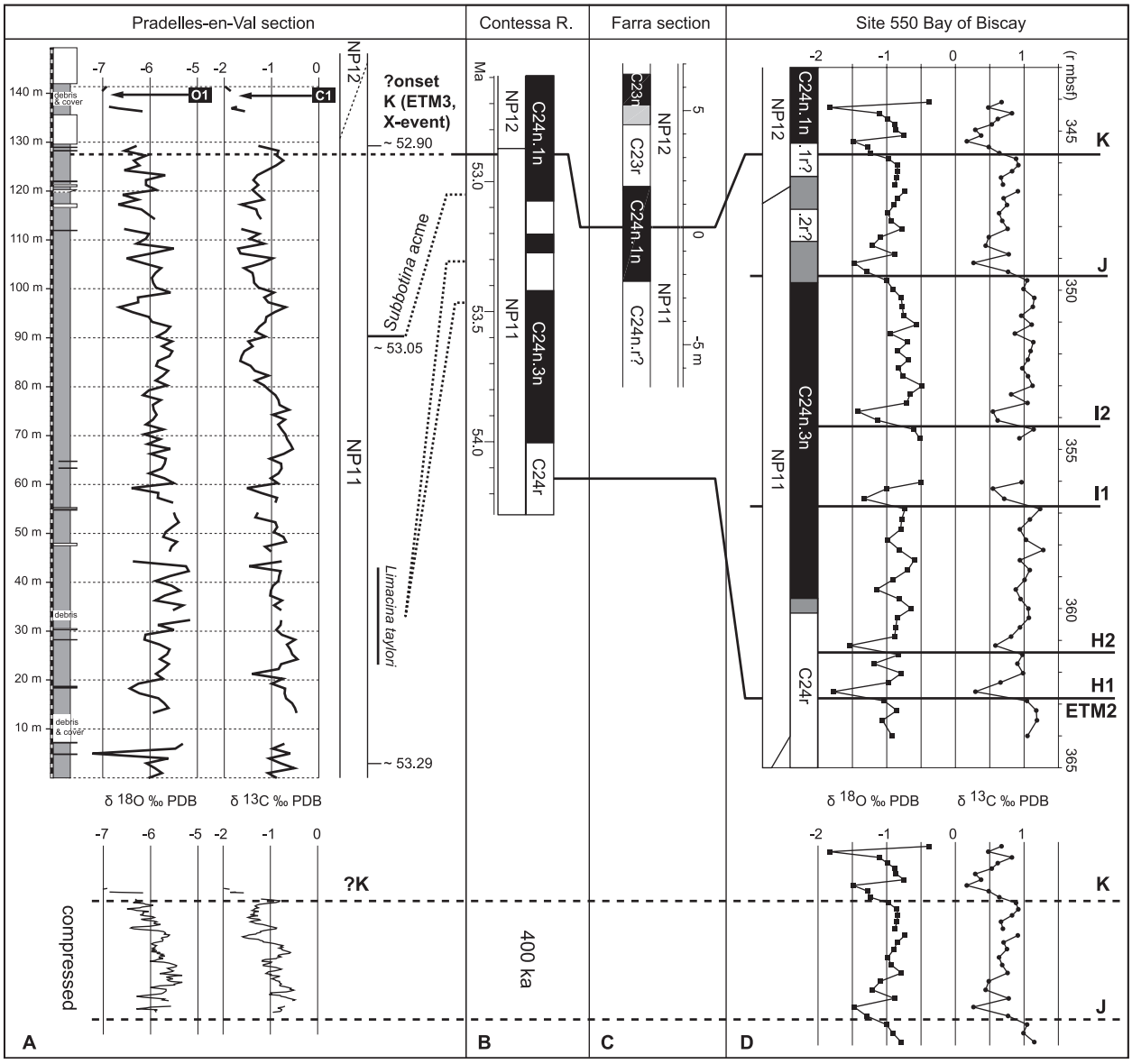

Fig. 10. Stable isotope record (bulk sediment; three point moving average = gray line) comparison between the Pradelles section and pelagic sites, position of CIEs/OIEs indicated (after **A** Fig. 8, **B** Galeotti et al. 2010, **C** Agnini et al. 2009 and **D** Cramer et al. 2003). Compressed section curve below (3 point moving average).

with values consistently hovering around –1.5‰ $\delta^{13}C$ throughout levels 107.3 to 124.3 m, and rising to > –1‰ $\delta^{13}C$ between 124.3 to 128.3 m.

The apparent absence of covariance between the $\delta^{13}C$-curve and the abundance of calcareous biota indicates no influence of the mass of the latter on the bulk sediment geochemistry throughout the section.

Strongly variable and very low $\delta^{18}O$ values are an indication of diagenetic overprint (e.g. Charisi and Schmitz 1995, Nelson and Smith 1996, Molina et al. 2003) like burial effects or meteoric impact. This may especially be expressed in the highly variable $\delta^{18}O$ values in various biofacies. It has to be noted though that large fluctuations in $\delta^{18}O$ also prevail in the deep-sea record (e.g. curves in Cramer et al. 2003). Since sample-by-sample covariance of $\delta^{13}C$ and $\delta^{18}O$ in the Pradelles-en-Val record occurs only sporadically (Fig. 5), the impact of a meteoric isotopic signature induced at a post-burial cementation stage is considered negligible (Corfield et al. 1991).

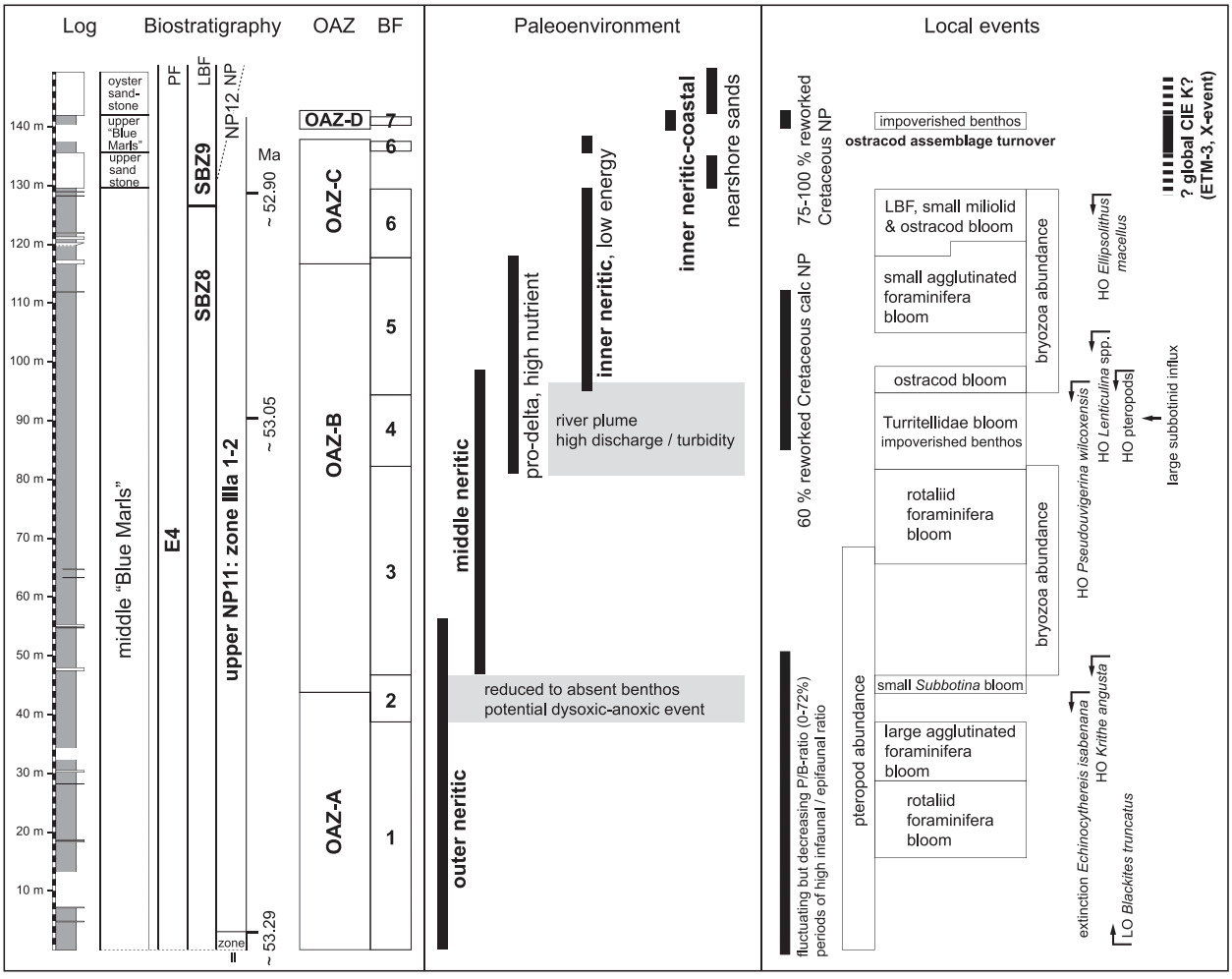

Fig. 11. Local events, lithostratigraphic, biostratigraphic and paleoenvironmental summary of the Pradelles-en-Val section.

5.4.2 Global early Eocene stable isotope background (Fig. 9, 10, Table 3)

Post-PETM whole rock bulk carbonate $\delta^{13}C$ (non-CIE) values at the pelagic DSDP Site 550 (Bay of Biscay) and the hemipelagic Contessa road section average +1‰ (Cramer et al. 2003, Galeotti et al. 2010) in calcareous nannoplankton zone NP11. Slightly higher values apply to southern Atlantic sites (Walvis ridge; +1.3 and +1.5‰; Stap et al. 2009) and the central Pacific (DSDP Site 577; +1.2‰ to 1.5‰; Cramer et al. 2003).

$\delta^{13}C$ values available from shallower-water settings tend to show larger variations and in general more negative whole rock values similar to the Pradelles-en-Val section. Depleted $\delta^{13}C$ values of shallow sequences relative to open ocean settings have been explained by the increased restriction or higher freshwater influx in marginal marine basins (Patterson and Walter 1994), coupled with reduced surface-water productivity and syndepositional diagenetic oxidation of increased organic detritus input during sea-level lowstands (Charisi and Schmitz 1995). The reworking of isotopic depleted organic-rich, uplifted hinterland sediments (Beck et al. 1995) may equally contribute to more depleted values in marginal settings (Höntzsch et al. 2011).

While post-PETM values from upper slope deposits of New Zealand (lower NP11; Nicolo et al. 2007) are still within the general range at an average of +1.3‰, whole-rock values from open marine shelf sediments at Gebel Duwi and Gebel Aweina (Egypt; NP10) vary between –2‰ and 0‰ (Schmitz et al. 1996). Values in-between the ETM2 and ETM3 CIEs from the Galala carbonate platform (Egypt) are similar, but may also be higher, ranging in different sections between –2‰ to 1‰ (Höntzsch et al. 2011). For the neritic

Table 3 Stable isotope value ranges and CIE minima per author.

Author	Locality	Setting	Values in bio-stratigraphic range	‰ $\delta^{13}C$ bulk ranges	‰ $\delta^{18}O$ bulk ranges	CIE in ‰ $\delta^{13}C$						
						PETM	ETM2	H2	I1	I2	J	ETM3
Agnini et al. 2009	Possagno	hemipelagic	NP11	0.5 to 1.0	n. a.	1.5	0.4	n. a.	?0.35		?0.27	?0.3
	Farra	hemipelagic	NP11	0.4 to –0.5	n. a.	n. a.	n. a.		n. a.	n. a.	n. a.	~0.65
Cramer et al. 2003	DSDP 550	pelagic	NP11	0.26 to 1.28	–1.78 to –0.49	1.2	0.9	0.4	0.7	0.6	0.7	0.75
	DSDP 577	pelagic	NP11	0.66 to 1.69	–1.02 to –0.08	n. a.	0.6	0.3	0.5	0.2	?0.35	0.66
Egger et al. 2005	Untersberg	lower bathyal	NP9-10	0.6 to 1.7	–2.5 to –1.5	?> 3.0	n. a.	n. a.	n. a.	n. a.	n. a.	n. a.
Galeotti et al. 2010	Contessa road	?hemipelagic	NP11	0.5 to 1.3	n. a.	2.1	0.7	n. a.	?0.5		n. a.	~0.5
Höntzsch et al. 2011	Galala platform	mid-ramp (log 4a)	NP10-11	0.5 to 1.5	n. a.	1.7	1.5	n. a.	1.0	n. a.	n. a.	1.6
Molina et al. 2003	Campo	neritic	NP10-11	–4.0 to 1.2	–6.2 to –1.7	?2.6	n. a.	n. a.	n. a.	n. a.	n. a.	n. a.
Nicolo et al. 2007	Mead stream	upper slope	lower NP11	~1.3	n. a.	2.5	1.0	0.2	0.75	n. a.	n. a.	n. a.
	Dee stream			~1.3	n. a.	2.4	0.8	0.2	0.6	0.25	n. a.	n. a.
Speijer & Morsi 2002	Gebel Duwi	middle neritic	NP9-10	–1.8 to 0	n. a.	4.5	n. a.	n. a.	n. a.	n. a.	n. a.	n. a.
Speijer et al. Morsi 2002	Gebel Aweina	outer neritic	NP9-10	–1.7 to 0	n. a.	1.5	n. a.	n. a.	n. a.	n. a.	n. a.	n. a.
Stap et al.	ODP 1263	pelagic, shallower	not available	~1.3 pre ETM2 ~1.3 post H2	n. a.	n. a.	1.6	0.6	n. a.	n. a.	n. a.	n. a.
2009 deeper	ODP 1267	pelagic,	not available	~1.5 pre ETM2 ~1.5 post H2	n. a.	n. a.	1.5	0.6	?0.25	n. a.	n. a.	n. a.
this study	Pradelles-en-Val	outer – inner neritic	upper NP11	–1.98 to –0.45	–7.22 to –5.15	local CIE in‰ $\delta^{13}C$ (C1-3)						
						BF1 0.8		BF4 1.0			BF6-7 1.2	

Campo section in the larger Aquitain Basin, whole-rock values from NP11 (only 6 samples) range between –0.5‰ and –4‰. They are though much more strongly influenced by diagenetic alteration (Molina et al. 2003) than the Pradelles-en-Val section,in which nearly all $\delta^{13}C$ values range between –1.5‰ and –0.5‰.

Comparable isotopic behaviour applies to the $\delta^{18}O$ values, but the curves tend to be more erratic than for $\delta^{13}C$ values (both pelagic and neritic settings). Pelagic values shift between –1‰ and –0.5‰ at the DSDP Sites 550, 577 and 1051A (e.g. Cramer et al. 2003).

Thus the general post-PETM whole rock isotopic signature of the Pradelles-en-Val section correlates well with (unaltered or only slightly altered) values from other neritic sections, and displays the characteristic negative offset of shallower marine records.

5.4.3 Correlation of the local stable isotope record (Fig. 10, 11)

Four global post-PETM isotopic excursions (I1 to K) come into consideration within the upper part of calcareous nannoplankton zone NP11 (Cramer et al. 2003). However, comparisons to pelagic sites are complicated by discrepancies in the biostratigraphic, magnetostratigraphic and orbital calibration between different localities. CIE J and/or K (X-event, ETM3) described by Cramer et al. (2003) may either be attributed to NP11 or NP12, whereas I1 and I2 are consistently situated within NP11. More recent publications agree on the position of CIE K straddling the boundary of NP11-12 (e.g. Agnini et al. 2009, Galeotti et al. 2010). A comparison of both $\delta^{18}O$ and $\delta^{13}C$ values from the Pradelles-en-Val section to comparable neritic early Ypresian localities is not possible due to the lack of published data.

Of the four global post-PETM isotopic excursions the most likely to be recorded in the time frame of the Pradelles-en-Val section are excursions J and K, based on local biostratigraphic constraints. As the onset of CIE K (= ETM3, X-event) just precedes or is very close to the NP11-12 boundary (see citations above), its position is most likely located within the uppermost part of the Pradelles-en-Val section of equivalent biostratigraphic age, where the negative isotopic values of O and C drop near simultaneously about 1.2‰ (local excursions C1 and O1). The distinct faunal shift (e.g. HO and LO of ostracod taxa in BF7/OAZ-D) within the microfossil assemblages in this interval probably relates to the global climatic perturbation during the ETM3, but may also be driven by local paleoecological changes (response to transgression-regression cycles, see Fig. 8). Biotic changes related to the ETM3 comparable to the ones in the wake of the PETM, though of lesser magnitude, have been reported by Agnini et al. (2009) for the northwestern Tethys margin.

The detection of the older CIE J is hampered by its lesser magnitude in the global isotopic record (e.g. Cramer et al. 2003, Site 577; see Fig. 10 and values in Table 3). A plausible position of J would be below BF1, based on the average sedimentation rates and the 400 kyr eccentricity cycle separating global CIE J and K, and thus just below the logged Pradelles-en-Val section. This is probably also indicated by the long term trend of the $\delta^{18}O$-curve in Fig. 4 and 6, showing one minimum at the top of the section, and hinting at another minimum just below the base.

6. Conclusions

The analysis of the high-resolution stratigraphic, microfossil and geochemical record of the Pradelles-en-Val section allows the following conclusions:

1. The Pradelles-en-Val section can be subdivided in seven distinct biofacies and four ostracod assemblage zones, confirming outer to middle neritic environments in the lower part and a subsequent shallowing up. A potential anoxic event is indicated in biofacies 2 by the decrease and subsequent near absence of benthic biota.
2. Calcareous nannofossil and larger benthic foraminifera data pinpoint the Pradelles-en-Val section in upper NP11 (subzones II, IIIa), up to probably basal NP12 (early to middle Ypresian) and shallow benthic zone SBZ8-9 respectively. The section has an approximate duration of about 0.4 Myr and average sediment accumulation rates of 32 cm/kyr.
3. At the top of the section, a negative $\delta^{13}C$- and $\delta^{18}O$-excursion of both ~ 1.2‰ occurs. Based on the biostratigraphy indicating this interval corresponds to the NP11-12 transition, these excursions could be tentatively linked to carbon isotope excursion K associated with Eocene Thermal Maximum 3 (ETM3). The distinct faunal shift within the microfossil assemblages in the latter biofacies could relate to the climatic perturbation induced by ETM3, or alternatively to local paleoecological changes. Further studies on time-equivalent local and global sections to clarify the impact of the ETM3 on shallow marine biota and isotopic record are needed.

Acknowledgements. We thank Ronald Janssen for determining the gastropod material and Arie Janssen for comments and identifications concerning the pteropods. Prof. Dr. M. Joachimski (GeoZentrum Nordbayern) is acknowledged for carrying out the stable isotope analysis. We thank two anonymous reviewers for their extensive and constructive reviews of the original manuscript. The project was funded by the Swiss National Science Foundation project No. PB FR22-116947 and supported by the KU Leuven Research Fund.

References

Afzal, J., Williams, M., Aldridge, R.J., 2009. Revised stratigraphy of the lower Cenozoic succession of the Greater Indus Basin in Pakistan. Journal of Micropalaeontology **28**(1), 7–23.

Agnini, C., Macrì, P., Backman, J., Brinkhuis, H., Fornaciari, E., Giusberti, L., Luciani, V., Rio, D., Sluijs, A., Speranza, F., 2009. An early Eocene carbon cycle perturbation at ~52.5 Ma in the Southern Alps: Chronology and biotic response. Paleoceanography **24**, 14 p., doi:10.1029/2008PA001649, 2009.

Alegret, L., Ortiz, S., 2006. Global extinction event in benthic foraminifera across the Paleocene/Eocene boundary at the Dababiya stratotype section. Micropaleontology **52**(5), 433–447.

Alegret, L., Ortiz, S., Arenillas, I., Molina, E., 2010. What happens when the ocean is overheated? The foraminiferal response across the Paleocene-Eocene Thermal Maximum at the Alamedilla section (Spain). Geological Society of America Bulletin **122**(9–10), 1616–1624.

Ali, J.R., King, C., Hailwood, E.A., 1993. Magnetostratigraphic calibration of early Eocene depositional sequences in the southern North Sea Basin. In: Hailwood, E.A., Kidd, R.B. (Eds.), High resolution stratigraphy. Geological Society, Special Publications **70**, 99–125.

Andreasson, F.P., Schmitz, B., 1996. Winter and summer temperatures of the early middle Eocene of France from Turritella $\delta^{18}O$ profiles. Geology **24**(12), 1067–1070.

Andreasson, F.P., Schmitz, B., 2000. Temperature seasonality in the early middle Eocene North Atlantic region: Evidence from stable isotope profiles of marine gastropod shells. Geological Society of America Bulletin **112**(4), 628–640.

Beck, R.A., Burbank, D.W., Sercombe, W.J., Olson, T.L., Khan, A.M., 1995. Organic carbon exhumation and global warming during the early Himalayan collision. Geology **23**(5), 387–390.

Berggren, W.A., Pearson, P.N., 2006. Tropical to subtropical planktonic foraminiferal zonation of the Eocene and Oligocene. Cushman Foundation Special Publication **41**, 29–40.

Berggren, W.A., Pearson, P.N., Huber, B.T., Wade, B.S., 2006. Taxonomy, biostratigraphy, and phylogeny of Eocene *Acarinina*. Cushman Foundation Special Publication **41**, 257–326.

Bernhard, 1986. Characteristic assemblages and morpjologies of benthic foraminifera from anoxic, organic-rich deposits: Jurassic through Holocene. Journal of Foraminiferal Research **16**(3), 207–215.

Bowen, G.J., Bralower, T.J., Delaney, M.L., Dickens, G.R., Kelly, D.C., Koch, P.L., Kump, L.R., Meng, J., Sloan, L.C., Thomas, E., 2006. Eocene hyperthermal event offers insight into greenhouse warming. Eos, Transactions, American Geophysical Union **87**(17), 165–167.

Breton, G., Vizcaïno, D., 1997. Astérides (Echinodermata) de l'Ilerdien moyen (Yprésien) des Corbières (Aude, France): systématique, relations paléobiogéographiques et évolutives. Bulletin de la Société d'Etudes Scientifiques de l'Aude **97**, 11–28.

Canudo, J.I., Molina, E., 1992. Planktic foraminiferal faunal turnover and bio-chronostratigraphy of the Paleocene-Eocene boundary at Zumaya (Northern Spain). Revista de la Sociedad Geológica de España **5**(1–2), 145–157.

Charisi, S.D., Schmitz, B., 1995. Stable ($\delta^{13}C$, $\delta^{18}O$) and strontium ($^{87}Sr/^{86}Sr$) isotopes through the Paleocene at Gebel Aweina, eastern Tethyan region. Palaeogeography, Palaeoclimatology, Palaeoecology **116**(1–2), 103–129.

Corfield, R.M., Cartlidge, J.E., Premoli Silva, I., Housley, R.A., 1991. Oxygen and carbon isotope stratigraphy of the Palaeogene and Cretaceous limestones in the Bottaccione Gorge and the Contessa Highway sections, Umbria, Italy. Terra Nova **3**, 414–422.

Cramer, B.S., Wright, J.D., Kent, D.V., Aubry, M.-P., 2003. Orbital climate forcing of $\delta^{13}C$ excursions in the late Paleocene-early Eocene (chrons C24n–C25n). Paleoceanography **18**(4), 25 p., doi:10.1029/2003PA000909.

Dedert, M., Stoll, H.M., Kroon, D., Shimizu, N., Kanamaru, K., Ziveri, P., 2012. Productivity response of calcareous nannoplankton to Eocene Thermal Maximum 2 (ETM2). Climate of the Past **8**, 977–993.

De Graciansky, P.-C., Hardenbol, J., Jacquin, T., Vail, P. (Eds.), 1998. Mesozoic and Cenozoic sequence stratigraphy of European basins. SEPM Special Publication **60**, 791p.

Dickens, G.R., 2009. Early Cenozoic hyperthermals: The sedimentary record of rapid global warming and massive carbon input. CSEG Recorder, February **2009**, 28–32.

Dominici, S., Kowalke, T., 2007. Depositional dynamics and the record of ecosystem stability: Early Eocene faunal gradients in the Pyrenean foreland, Spain. Palaios **22**, 268–284.

Dunkley Jones, T., Ridgwell, A., Lunt, D.J., Maslin, M.A., Schmidt, D.N., Valdes, P.J., 2010. A Palaeogene perspective on climate sensitivity and methane hydrate instability. Philosophical Transactions of the Royal Society A **368**, 2395–2415.

Dupuis, C., Aubry, M.-P., Steurbaut, E., Berggren, W.A., Ouda, K., Magioncalda, R., Cramer, B.S., Kent, D.V., Speijer, R.P., Heilmann-Clausen, C., 2003. The Dababiya Quarry Section: Lithostratigraphy, clay mineralogy, geochemistry and paleontology. Micropaleontology, **49**(suppl. 1), 41–59.

Egger, H., Homayouna, M., Huber, H., Rögl, F., Schmitz, B., 2005. Early Eocene climatic, volcanic, and biotic events in the northwestern Tethyan Untersberg section, Austria. Palaeogeography, Palaeoclimatology, Palaeoecology **217**, 243–264.

Ernst, S., Bours, R., Duijnstee, I., van der Zwaan, B., 2005. Experimental effects of an organic matter pulse and oxygen depletion on a benthic foraminiferal shelf community. Journal of Foraminiferal Research **35**(3), 177–197.

Ernst, S.R., Guasti, E., Dupuis, C., Speijer, R.P., 2006. Environmental perturbation in the southern Tethys across the Paleocene/Eocene boundary (Dababiya, Egypt): Foraminiferal and clay mineral records. Marine Micropaleontology **60**(1), 89–111.

Galeotti, S., Krishnan, S., Pagani, M., Lanci, L., Gaudio, A., Zachos, J.C., Monechi, S., Morelli, G., Lourens, L., 2010. Orbital chronology of Early Eocene hyperthermals from the Contessa Road section, central Italy. Earth and Planetary Science Letters **290**(1–2), 192–200.

Geel, T., 2000. Recognition of stratigraphic sequences in carbonate platform and slope deposits: empirical models based on microfacies analysis of Palaeogene deposits in southeastern Spain. Palaeogeography, Palaeoclimatology, Palaeoecology **155**(3–4), 211–238.

Gély, J.P., Sztrákos, K., 2000. L'évolution paléogéographique et géodynamique du bassin aquitain au paléogène: Enregistrement et datation de la tectonique pyrénéenne. Géologie de la France **2**, 31–57.

Giusberti, L., Rio, D., Agnini, C., Backman, J., Fornaciari, E., Tateo, F., Oddone, M., 2007. Mode and tempo of the Paleocene Eocene thermal maximum in an expanded section from the Venetian pre-Alps. Geological Society of America Bulletin **119**, 391–412.

Höntzsch, S., Scheibner, C., Guasti, E., Kuss, J., Marzouk, A.M., Rasser, M.W., 2011. Increasing restriction of the Egyptian shelf during the Early Eocene? – New insights from a southern Tethyan carbonate platform. Palaeogeography, Palaeoclimatology, Palaeoecology **302**, 349–366.

Janssen, A.W., King, C., 1988. Planktonic mollusks (Pteropoda). In: Vinken, R. (comp.), The northwest European Tertiary Basin. Results of the IGCP Project No. 124, Geologisches Jahrbuch **A100**, 356–368.

Kapellos, C., Schaub, H., 1973. Zur Korrelation von Biozonierungen mit Grossforaminiferen und Nannoplankton um Paläogen der Pyrenäen. Eclogae Geologicae Helvetiae **66**(3), 687–737.

Kennet, J.P., Stott, L.D., 1991. Abrupt deep-sea warming, palaeoeanographic changes and benthic extinctions at the end of the Palaeocene. Nature **353**, 225–229.

King, C., 1991. Stratigraphy of the London Clay Formation (early Eocene) in the Hampshire Basin. PhD Thesis, School of Geology, Kingston Polytechnic, 320 p.

Latal, C., Piller, W.E., Harzhauser, M., 2004. Palaeoenvironmental reconstructions by stable isotopes of Middle Miocene gastropods of the Central Paratethys. Palaeogeography, Palaeoclimatology, Palaeoecology **211**(1–2), 157–169.

Leon-Rodriguez, L., Dickens, G.R., 2010. Constraints on ocean acidification associated with rapid and massive carbon injections: The early Paleogene record at ocean drilling program site 1215, equatorial Pacific Ocean. Palaeogeography, Palaeoclimatology, Palaeoecology **298**(3–4), 409–420.

Levin, L., 2003. Oxygen minimum zone benthos: adaption and community response to hypoxia. Oceanography and Marine Biology: an Annual Review **41**, 1–45.

Lezaud, L., Massieux, M., Toumarkine, M., 1969. Prinipaux resultats d'une étude des foraminifères pélagiques et du nannoplancton calcaire du Nummulitique des Corbières septentrionales et du Mont Cayla (Aude). Bulletin de la Société d'histoire naturelle de Toulouse **105**(1–2), 121–135.

Lourens, L.J., Sluijs, A., Kroon, D., Zachos, J.C., Thomas, E., Röhl, U., Bowles, J., Raffi, I., 2005. Astronomical pacing of late Palaeocene to early Eocene global warming events. Nature **435**, 1083–1087.

Luterbacher, H., Ali, J.R., Brinkhuis, H., Gradstein, F.M., Hooker, J.J., Monechi, S., Ogg, J.G., Powell, J., Röhl, U., Sanfilippo, A., Schmitz, B., 2004. The Paleogene period. In: Gradstein, F.M., Ogg, J.G., Smith, A.G. (Eds.), A geologic time scale 2004. Cambridge University Press, Cambridge, 384–408.

Marshall, J.D., 1992. Climatic and oceanographic isotopic signals from the carbonate rock record and their preservation. Geological Magazine **129**(2), 143–160.

Martini, E., 1971. Standard Tertiary and Quaternary calcareous nannoplankton zonation. In: Farinacci, A. (Ed.), Proceedings of the 2nd Planktonic Conference, Roma, Tecnoscienza **2**, 739–785.

Martín-Martín, M., Rey, J., Alcala-Garcia, F.J., Tosquella, J., Deramond, J., Lara-Corona, E., Duranthon, F., Antoine, P.O., 2001. Tectonic controls on the deposits of a foreland basin: An example from the Eocene Corbières-Minervois basin, France. Basin Research **13**, 419–433.

Massieux, M., 1973. Micropaléontologie stratigraphique de l'Éocène des Corbières septentrionales (Aude). Éditions du Centre national de la recherche scientifique, 143 p.

Molina, E., Angori, E., Arenillas, I., Brinkhuis, H., Crouch, E.M., Luterbacher, H., Monechi, S., Schmitz, B., 2003. Correlation between the Paleocene/Eocene boundary and the Ilerdian at Campo, Spain. Revue de Micropaléontologie **46**(2), 95–109.

Molina, E., Canudo, J.I., Guernet, C., Mcdougall, K., Ortiz, N., Pascual, J.O., Pares, J.O., Samso, J.M., Serra-Kiel, J., Tosquella, J., 1992. The stratotype Ilerdian revisited: integrated stratigraphy across the Paleocene/Eocene boundary. Revue de Micropaléontologie **35**(2), 143–156.

Moodley, L., Hess, C., 1992. Tolerance of infaunal benthic foraminifera for low and high oxygen concentrations. – Biological Bulletin **183**(1), 94–98.

Nelson, C.S., Smith, A.M., 1996. Stable oxygen and carbon isotope compositional fields for skeletal and diagenetic components in New Zealand Cenozoic nontropical carbonate sediments and limestones: a synthesis and review. New Zealand Journal of Geology and Geophysics **39**(1), 93–107.

Nicolo, M.J., Dickens, G.R., Hollis, C.J., Zachos, J.C., 2007. Multiple early Eocene hyperthermals: Their sedimentary expression on the New Zealand continental margin and in the deep sea. Geology **35**(8), 699–702.

Oertli, H.J., 1960. Évolution d'une espece d'*Echinocythereis* dans le Lutétien du Rio Isabena (Prov, Huesca, Espagne). Revue de Micropaléontologie **3**, 147–166.

Pardo, A., Keller, G., Oberhänsli, H., 1999. Paleoecologic and paleoceanographic evolution of the tethyan realm during the Paleocene-Eocene transition. Journal of Foraminiferal Research **29**(1), 37–57.

Patterson, W.P., Walter, L.M., 1994. Syndepositional diagenesis of modern platform carbonates: Evidence from isotopic and minor element data. Geology **22**(2), 127–130.

Perch-Nielsen, K., 1985. Cenozoic calcareous nannofossils. In: Bolli, H.M., Saunders, J.B., Perch-Nielsen, K. (Eds.), Plankton Stratigraphy. Cambridge Earth Science Series **11**, 427–554.

Petrizzo, M.R., 2007. The onset of the Paleocene-Eocene Thermal Maximum (PETM) at Sites 1209 and 1210 (Shatsky Rise, Pacific Ocean) as recorded by planktonic foraminifera. Marine Micropaleontology **63**(3–4), 187–200.

Plaziat, J.-C., 1981. Late Cretaceous to Late Eocene palaeogeographic evolution of southwest Europe. Palaeogeography, Palaeoclimatology, Palaeoecology **36**(3–4), 263–320.

Pujalte, V., Baceta, J.I., Schmitz, B., Orue-Extebarria, X., Payros, A., Bernaola, G., Apellaniz, E., Caballero, F., Robador, A., Serra-Kiel, J., Tosquella, J., 2009. Redefinition of the Ilerdian Stage (early Eocene). Geologica acta **7**(1–2), 177–194.

Purton, L.M.A., Brasier, M.D., 1999. Giant protist Nummulites and its Eocene environment: Life span and habitat insights from $\delta^{18}O$ and $\delta^{13}C$ data from Nummulites and Venericardia, Hampshire basin, UK. Geology **27**(8), 711–714.

Rasser, M.W., Scheibner, C., Mutti, M., 2005. A paleoenvironmental standard section for early Ilerdian tropical carbonate factories (Corbières, France; Pyrenees, Spain). Facies **51**, 217–232.

Saraswati, P.K., Kumar, A., Patra, P.K., Banerji, R.K., 1997. Isotopic paleobiology of some Tertiary larger foraminifera from Kutch, India. Journal of Foraminiferal Research **27**(1), 69–74.

Schaub, H., 1981. Nummulites et assilines de la Téthys paléogène. Taxinomie, phylogenèse et biostratigraphie. Schweizerische Paläontologische Abhandlungen **104–106**, 1–236 (+ atlas).

Scheibner, C., Rasser, M.W., Mutti, M., 2007. The Campo section (Pyrenees, Spain) revisited: Implications for changing benthic carbonate assemblages across the Paleocene-Eocene boundary. Palaeogeography, Palaeoclimatology, Palaeoecology **248**(1–2), 145–168.

Scheibner, C., Speijer, R.P., 2009. Recalibration of the Tethyan shallow-benthic zonation across the Paleocene-Eocene boundary: the Egyptian record. Geologica Acta **7**(1–2), 195–214.

Scheibner, C., Speijer, R.P., Marzouk, A.M., 2005. Turnover of larger foraminifera during the Paleocene-Eocene Thermal Maximum and paleoclimatic control on the evolution of platform ecosystems. Geology **33**(6), 493–496.

Schmitz, B, Heilmann-Clausen, C., King, C., Steurbaut, E., Andreasson, F.P., Corfield, R.M., Cartlidge, J.E., 1996. Stable isotope and biotic evolution in the North Sea during the early Eocene: the Albæk Hoved section, Denmark. Special Publication of the Geological Society of London **101**(1), 275–306.

Schmitz, B., Speijer, R.P., Aubry, M.-P., 1996. Latest Paleocene benthic extinction event on the southern Tethyan shelf (Egypt): Foraminiferal stable isotopic ($\delta^{13}C$, $\delta^{18}O$) records. Geology **24**(4), 347–350.

Serra-Kiel, J., Canudo, J.I., Dinares, J., Molina, E., Ortiz, N., Pascual, J.O., Samso, J.M., Tosquella, J., 1994. Cronoestratigrafía de los sedimentos marinos del Terciario inferior de la Cuenca de Graus-Tremp (Zona Central Surpirenaica). Revista de la Sociedad Geológica de España **7**(3–4), 273–297.

Serra-Kiel, J., Hottinger, l., Caus, E., Drobne, K., Ferràndez, C., Jauhri, A.K., Less, G., Pavlovec, R., Pignatti, J., Samsó, J.M., Schaub, H., Sirel, E., Strougo, A., Tambareau, Y., Tosquella, J., Zakrevskaya, E., 1998. Larger foraminiferal biostratigraphy of the Tethyan Paleocene and Eocene. Bulletin de la Societé géologique de France **169**(2), 281–299.

Speijer, R.P., Morsi, A.-M.M., 2002. Ostracode turnover and sea-level changes associated with the Paleocene-Eocene thermal maximum. Geology **30**(1), 23–26.

Speijer, R.P., Schmitz, B., Aubry, M.P., Charisi, S.D., 1995. The latest Paleocene benthic extinction event: Punctuated turnover in outer neritic foraminiferal faunas from Gebel Aweina, Egypt. Israel Journal of Earth Sciences **44**, 207–222.

Speijer, R.P., van der Zwaan, G.J., Schmitz, B., 1996. The impact of Paleocene/Eocene boundary events on middle neritic benthic foraminiferal assemblages from Egypt. Marine Micropaleontology **28**(2), 99–132.

Stap, L., Sluijs, A., Thomas, E., Lourens, L., 2009. Patterns and magnitude of deep sea carbonate dissolution during Eocene Thermal Maximum 2 and H2, Walvis Ridge, southeastern Atlantic Ocean. Paleoceanography **24**, 13 p., doi:10.1029/2008PA001655.

Stassen, P., Steurbaut, E., Morsi, A.-M.M., Schulte, P., Speijer, R.P., 2012. Biotic impact of Eocene thermal maximum 2 in a shelf setting (Dababiya, Egypt). Austrian Journal of Earth Sciences **105**(1), 154–160.

Steurbaut, E., 1991. Ypresian calcareous nannoplankton biostratigraphy and palaeogeography of the Belgian Basin. In: Dupuis, C., De Coninck, J., Steurbaut, E. (Eds.): The Ypresian stratotype. Bulletin van de Belgische Vereniging voor Geologie **97**(3–4), 251–285.

Steurbaut, E., 1998. High-resolution holostratigraphy of Middle Paleocene to Early Eocene strata of Belgium and adjacent areas. Palaeontographica Abt. A **247**(5–6), 91–156.

Steurbaut, E., 2011. New calcareous nannofossil taxa from the Ypresian (Early Eocene) of the North Sea Basin and

the Turan Platform in West Kazakhstan. Bulletin de l'Institut royal des Sciences naturelles de Belgique, Sciences de la Terre **81**, 247–277.

Steurbaut, E., King, C., 1994. Integrated stratigraphy of the Mont-Panisel borehole section (151E340), Ypresian (Early Eocene) of the Mons Basin, SW Belgium. Bulletin van de Belgische Vereniging voor Geologie **102**(1–2), 175–202.

Tambareau, Y., 1994. Paleocene/Eocene boundary in the platform deposits of the northern Pyrenees. Bulletin de la Société belge de Géologie **103**(3–4), 293–299.

Tambareau, Y., Crochet, B., Villatte, J., Deramond, J., 1995. Evolution tectono-sédimentaire du versant nord des pyrénées centre-orientales au paléocène et à l'Eocène inférieur. Bulletin de la Societé géologique de France **166**(4), 375–387.

Thomas, E., 1989. Development of Cenozoic deep-sea benthic foraminiferal faunas in Antarctic waters. Geological Society Special Publication **47**, 283–296.

Thomas, E., 2003. Extinction and food at the seafloor: A high-resolution benthic foraminiferal record across the initial Eocene Thermal Maximum, Southern Ocean Site 690. Geological Society of America Special Paper **369**, 319–332.

Thomas, E., Barrera, E., Hamilton, N., Huber, B.T., Kennet, J.P., O'Connel, S.B., Pospichal, J.J., Spieß, V., Stott, L.D., Wei, W., Wise, S.W. Jr., 1990. Upper Cretaceous-Paleogene stratigraphy of Sites 689 and 690, Maud Rise (Antarctica). Proceedings of the Ocean Drilling Program, Scientific Results **113**, 901–914.

Tyson, R.V., Pearson, T.H., 1991. Modern and ancient continental shelf anoxia: an overview. Geological Society of London Special Publication **58**, 1–24.

Vandenberghe, N., Hilgen, F.J., Speijer, R.P., 2012. The Paleogene period. In: Gradstein, F.M., Ogg, J.G., Schmitz, M., Ogg, G. (Eds.), The geologic time scale 2012. Elsevier, Amsterdam, 855–9218.

Wachter, E., Hayes, J.M., 1985. Exchange of oxygen isotopes in carbon-dioxide – phosphoric acid systems. – Chemical Geology **52**, 365–374.

Wade, B.S., Pearson, P.N., Berggren, W.A., Pälike, H., 2011. Review and revision of Cenozoic tropical planktonic foraminiferal biostratigraphy and calibration to the geomagnetic polarity and astronomical time scale. Earth-Science Reviews **104**(1–3), 111–142.

Waite, R., Strasser, A., 2011. A comparison of recent and fossil large, high-spired gastropods and their environments: the Nopparat Thara tidal Xat in Krabi, South Thailand, versus the Swiss Kimmeridgian carbonate platform. Facies **57**, 223–248.

Westerhold, T., Röhl, U., Laskar, J., 2012. Time scale controversy: Accurate orbital calibration of the early Paleogene. Geochemistry, Geophysics, Geosystems **13**(6), 1–19.

Willems, W.A.E., 1982. Microfossil assemblages, zonations and planktonic datum levels in the leper Formation (Ypresian S.S., Early Eocene) in Belgium. Belg. Geol. Dienst, Prof. Paper 194, 1–16.

Zachos, J., Pagani, M., Sloan, L., Thomas, E., Billups, K., 2001. Trends, Rhythms, and Aberrations in Global Climate 65 Ma to Present. Science **292**, 686–693.

Zachos, J.C., Röhl, U., Schellenberg, S.A., Sluijs, A., Hodell, D.A., Kelly, D.C., Thomas, E., Nicolo, M., Raffi, I., Lourens, L.J., McCarren, H., Kroon, D., 2005. Rapid acidification of the ocean during the Paleocene-Eocene thermal maximum. Science **308**, 1611–1615.

Manuscript received: June 25, 2012; rev. version accepted: August 23, 2013.